Quaternary Science Reviews 287 (2022) 107564

Contents lists available at ScienceDirect

Quaternary Science Reviews

journal homepage: www.elsevier.com/locate/quascirev

Laurentide Ice Sheet extent over the last 130 thousand years traced by the Pb isotope signature of weathering inputs to the Labrador Sea

Rebecca L. Parker [a, *, 1], Gavin L. Foster [b], Marcus Gutjahr [c], Paul A. Wilson [b], Kate L. Littler [a], Matthew J. Cooper [b], Agnes Michalik [b], James A. Milton [b], Kirsty C. Crocket [d], Ian Bailey [a]

[a] Camborne School of Mines, College of Engineering, Mathematics & Physical Sciences, University of Exeter, Penryn Campus, Treliever Road, Penryn, TR10 9FE, UK
[b] School of Ocean and Earth Science, University of Southampton, Waterfront Campus, European Way, Southampton, SO14 3ZH, UK
[c] GEOMAR Helmholtz Centre for Ocean Research Kiel, Wischhofstraße 1–3, 24148, Kiel, Germany
[d] Dounreay Site Restoration Ltd, Dounreay, Thurso, Scotland, UK

ARTICLE INFO

Article history:
Received 17 September 2021
Received in revised form
7 April 2022
Accepted 10 May 2022
Available online xxx

Handling Editor: Dr A. Voelker

Keywords:
Quaternary
Paleoceanography
North Atlantic
Last Glacial Cycle
Labrador Current
Continental runoff
Chemical weathering
Rare earth elements
Fe–Mn oxyhydroxides

ABSTRACT

Understanding the history of continental ice-sheet growth on North America, and in particular that of the Laurentide Ice Sheet (LIS), is important for palaeoclimate and sea-level reconstructions. Information on ice-sheet extent pre-dating the Last Glacial Maximum (LGM) is heavily reliant, though, on the outputs of numerical models underpinned by scant geological data. Important aspects of LIS history that remain unresolved include the timing of its collapse during Termination 2, the first time that it expanded significantly during the Last Glacial Cycle, and whether its volume was significantly reduced during marine isotope stage (MIS) 3. To address these issues and more, we present authigenic iron-manganese (Fe–Mn) oxyhydroxide-derived high-resolution records of Pb isotope data and associated rare earth element profiles for samples spanning the past ~130 kyr from northwest North Atlantic Labrador Sea, IODP Site U1302/3. We use these new data to track chemical weathering intensity and solute flux to the Labrador Sea associated with LIS extent on the adjacent highly radiogenic (high Pb isotope composition) North American Superior Province (SP) craton since the Penultimate Glacial Maximum (PGM). Our new records show that relatively high (radiogenic) values characterise warm marine isotope stages (MIS) 5, 3 and 1 and the lowest (most unradiogenic) values occurred during cold stages MIS 6, 4 and 2. The radiogenic Pb isotope excursion associated with Termination 2 is short-lived relative to the one documented for Termination 1, suggesting that LIS retreat during the PGM was relatively fast compared to the LGM and that its collapse during the last interglacial occurred ~125 ka. Highly radiogenic inputs to the Labrador Sea during MIS 5d-a, ~116–71 ka, most likely reflect a spin-up in Labrador Current vigour, incipient glaciation and renewed glacial erosion of high grounds of the eastern SP craton by localised wet-based ice-caps. A large decrease in Pb isotope values towards unradiogenic LGM-like compositions between ~75–65 ka across the MIS 5/4 transition likely reflects a slow-down in Labrador Current vigour, an increase in subaerial deposition of aeolian dust and a significant advance of the LIS across Hudson Bay caused a strong reduction or even abandonment of Pb sourcing from the SP. The relatively radiogenic Pb isotope composition of bottom-waters bathing our study site during MIS 3, 57–29 ka, is unlikely to support a recently proposed major reduction in LIS extent for this time. Instead, we argue these values are better explained by southern Greenland Ice Sheet retreat, increased chemical weathering of the Ketelidian Mobile Belt and subsequent Pb runoff from Greenland.

1. Introduction

The growth and decay of continental ice sheets has resulted in major fluctuations in global sea-level during the Quaternary (Rohling et al., 2014). Accurate reconstructions of past ice-sheet

* Corresponding author.
E-mail address: rebecca.parker1@unsw.edu.au (R.L. Parker).
[1] Now at: Chronos ^{14}Carbon-Cycle Facility, Mark Wainwright Analytical Centre, University of New South Wales, Sydney, NSW 2052, Australia.

https://doi.org/10.1016/j.quascirev.2022.107564

extent are necessary to understand the cause and timing of glacial terminations, rates of sea-level change and ice-sheet-ocean-atmosphere interactions. Knowledge of where ice-sheets grew during past glacials facilitates a firmer understanding of factors that drive their mass balance (e.g., astronomical cycles, atmospheric pCO_2 and associated feedbacks) and is also required to correct interglacial sea-level reconstructions accurately for glacial isostatic adjustment (GIA; so crustal loading and unloading) when ice-sheets grow or melt (e.g., Dendy et al., 2017). Yet we have only a rudimentary understanding of northern hemisphere continental ice-sheet histories prior to the Last Glacial Maximum (LGM), especially for the largest of these ice sheets, the North American Ice Sheet complex.

It has been shown that GIA-based corrections of Last Interglacial (MIS 5e, ~129–116 ka) sea-level records are highly sensitive to uncertainties in the distribution of Northern Hemisphere ice-sheets during preceding glacial maxima to the order of up to ~5 m (Dendy et al., 2017; Dwyer et al., 2021), a figure equivalent to the lower-end estimate and range of sea-level rise reported for this interglacial ($+6.6 \pm 2$ m; Kopp et al., 2013; Hibbert et al., 2016). Yet GIA models used to correct MIS 5e records for such factors mainly assume LGM ice-sheet distributions and volumes for the Northern Hemisphere during the PGM (~155–140 ka) and older glacial maxima (Dendy et al., 2017). Multiple lines of indirect evidence suggest, however, that the North American Ice Sheet complex during the PGM may have been considerably smaller than its LGM counterpart (e.g., Potter and Lambeck, 2003; Svendsen et al., 2004; Rabineau et al., 2006; Colleoni et al., 2011, 2016; Wainer et al., 2017; Rohling et al., 2017). Uncertainty in our knowledge of the North American Ice Sheet complex history is not just restricted to the PGM and older times. Our understanding, for instance, of when a large North American Ice Sheet Complex first grew during the Last Glacial Cycle (LGC) is poorly constrained by empirical data (compare Batchelor et al. (2019) to Pico et al. (2017)).

Considerable debate also exists about the extent of North American Ice Sheet complex reduction during the LGC warm interstadial MIS 3, ~29–57 ka (e.g., Pico et al., 2017; Dalton et al., 2019; Miller and Andrews, 2019; Gowan et al., 2021; Kerr et al., 2021). Uncertainty in MIS 3 ice-sheet extent is rooted in the sparsity of well dated terrestrial glaciomorphological evidence of pre-LGM age (e.g., Miller and Andrews, 2019). Much of our knowledge of the history of the North American Ice Sheet complex prior to the LGM is thus reliant on either numerical modelling experiments (e.g., Lambeck et al., 2006, 2010, 2017; Abe-Ouchi et al., 2013; de Boer et al., 2014; Colleoni et al., 2016) or indirect sedimentological evidence from glacially-derived terrigenous sediments deposited in marine ice-proximal Quaternary settings (e.g., Hemming, 2004; Hodell et al., 2008; Bailey et al., 2013; Lang et al., 2014). One proxy that has great potential to reveal important new insights into these issues is the Pb isotope composition of oceanic waters recorded in the Fe–Mn oxyhydroxide fraction of marine sediments. Owing to the particle-reactive nature and short seawater residence time of Pb (20–30 years), the Pb isotope compositions of authigenic Fe–Mn oxyhydroxides have been proposed to track regional weathering intensity and solute flux associated with glacial extent on adjacent continental landmasses (e.g., Crocket et al., 2012; Foster and Vance, 2006; Gutjahr et al., 2009; Kurzweil et al., 2010; Süfke et al., 2022). A short Pb isotope record from Integrated Ocean Drilling Program (IODP) Site U1302/3, recovered from North Atlantic Orphan Knoll proximal to northeast America, is most unradiogenic (so is characterised by its lowest $^{206}Pb/^{204}Pb$, $^{207}Pb/^{204}Pb$ and $^{208}Pb/^{204}Pb$) during the LGM and becomes more radiogenic (so increases) in response to increased continental chemical weathering of highly reactive glacial debris as the Laurentide Ice Sheet (LIS) retreated in the Hudson Bay region of northeast North America during the last deglacial (Crocket et al., 2012). Yet, this record, and other available North American-proximal Pb isotope Fe–Mn oxyhydroxide datasets (e.g., Gutjahr et al., 2009; Kurzweil et al., 2010; Süfke et al., 2022) are currently temporally limited to the past ~37 kyr.

To improve our understanding of LIS extent over the past ~130 kyr, we present new authigenic Fe–Mn oxyhydroxide-derived Pb isotope and rare earth element profiles of 87 samples from IODP Site U1302/3 reaching back to MIS 6. We examine the history of change in this new Pb isotope record and discuss the significance of its variability over this time in terms of LIS evolution.

2. Background

2.1. How are changes in Fe–Mn oxyhydroxide-derived Pb isotope ratios from site U1302/3 related to changes in ice-sheet extent on North America?

The Pb isotope composition of seawater bathing Orphan Knoll in the geological past was controlled by input from three main sources – the Mid Atlantic Ridge, the adjacent continents through chemical weathering and runoff and dust generation and its subaerial deposition in the Labrador Sea (Frank, 2002; Klemm et al., 2007). Given the high particle reactivity of Pb (Henderson and Maier-Reimer, 2002), an influence from chemical weathering and runoff of continental landmasses further afield than North America and Greenland seems unlikely for this region of the North Atlantic Ocean.

The Pb isotope composition of seawater can be determined by analysing the authigenic fraction of marine sediments. Lead has four naturally occurring isotopes. Three of these (^{206}Pb, ^{207}Pb ^{208}Pb) are the radiogenic daughter products of ^{238}U ($t_{1/2} = 4.5$ Ga; ^{206}Pb), ^{235}U ($t_{1/2} = 704$ Ma; ^{207}Pb), or ^{232}Th ($t_{1/2} = 14$ Ga; ^{208}Pb) respectively, while the other one (^{204}Pb) is a stable isotope. In our study we focused on using $^{206}Pb/^{204}Pb$, $^{207}Pb/^{204}Pb$ and $^{208}Pb/^{204}Pb$ ratios to track the Pb isotope composition of seawater bathing our study site. Due to the origin of the numerator isotope from U and Th decay, relatively high values for these ratios are described as being radiogenic, whereas low isotopic ratios are described as unradiogenic. Crocket et al. (2012) proposed that the relatively unradiogenic Pb isotope values bathing U1302/3 during LGM (~19.2 $^{206}Pb/^{204}Pb$) predominantly reflect a reduction in North American chemical weathering and runoff under a spatially extensive LIS and a dominance of a dust and Mid-Atlantic Ridge Pb isotope signal. They further argue that the subsequent trend towards more radiogenic values from ~19 ka records increased continental weathering intensity on these landmasses as well as increased runoff during Termination 1 as these ice sheets retreated under a warming climate. The peak radiogenic values obtained during the early Holocene (~8 ka, ~20.3 $^{206}Pb/^{204}Pb$) are attributed by these authors to incongruent weathering of highly reactive weakly chemically altered glacial debris exposed following ice-sheet retreat. In this model, the decay towards unradiogenic values of ~19.6 $^{206}Pb/^{204}Pb$ from ~7 ka is suggested to reflect a reduction in weathering intensity and release of unradiogenic Pb as the exposure age of this glacial debris increased and its supply was diminished (see also Harlavan et al., 1998; Foster and Vance, 2006). Crocket et al. (2012) argued that incongruent weathering processes must have a major control on the Pb isotopic composition of seawater bathing U1302/3 over the past ~37 ka because the values recorded are much too radiogenic to be controlled by regional variations in the chemical weathering of continental crust. This assertion is based on two observations: (1) the Pb isotope composition of U1302/3 detrital sediments, which may provide a well-mixed measure of the bulk composition of the potential

weathering source(s) from the adjacent continents, is much less radiogenic (~16–17 $^{206}Pb/^{204}Pb$) than the seawater signal (~19–21 $^{206}Pb/^{204}Pb$); and (2) a lack of co-variance exists between authigenic and detrital Pb isotope ratios at this site (Crocket et al., 2012).

Blaser et al. (2020) suggest, however, that the Pb isotope composition of detrital sediments at U1302/3 is much less radiogenic than the authigenic record because outside of Heinrich (H) events the authigenic radiogenic Pb signal recorded at Orphan Knoll must be dominated by dissolved and colloidal transport and subsequent scavenging into deep water and not terrigenous inputs. Recent laboratory experiments and observations from an enclosed Alpine lake challenge the notion that incongruent weathering can account for highly radiogenic Pb isotope ratios reported for U1302/3 during Termination (T) 1 and the early Holocene (see Dausmann et al., 2019; Süfke et al., 2019). Any incongruent weathering signal may take tens of thousands of years to decay (Harlavan et al., 1998; Süfke et al., 2019), which does not match the timescale of change observed during the Holocene at Orphan Knoll (~5 kyr) and elsewhere (e.g., Süfke et al., 2019). Instead, Blaser et al. (2020) argue that changing provenance may be a key factor. In other words, the Pb isotope signal at Orphan Knoll could also be generated by continental runoff transporting a congruent chemical weathering signal to the Labrador Sea and NW Atlantic. Through reference to a compilation of whole-rock Pb isotope data for circum-North Atlantic cratons assembled by Fagel et al. (2002), they suggest that the only regional continental source with Pb isotope ratios high enough to explain the variability in the U1302/3 Pb isotope record is the Superior Province (SP) of the Canadian Shield (mean $^{206}Pb/^{204}Pb = 25.7$, median $^{206}Pb/^{204}Pb = 22.7$; Table 1). During the LGM, the SP formed a central part of the foundation of the LIS south and east of Hudson Bay (Figs. 1 and 2). Today, the dissolved transport products of SP craton continental runoff are routed to the Labrador Sea through Hudson Bay and its straits (see hatched area in Fig. 1). This source area of Pb would have been significantly diminished, however, when Hudson Straits was cut off from the Labrador Sea by advance of the LIS in northeast North America during the LGM, resulting in relatively unradiogenic seawater Pb isotope ratios at Site U1302/3. In this interpretation, the most radiogenic ratios characteristic of bottom waters bathing U1302/3 during T1 and the early Holocene are attributed to enhanced supply of dissolved and colloidal radiogenic weathered material from the SP craton exposed following LIS retreat (Blaser et al., 2020).

2.2. Updating our understanding of the isotope composition of regional sources of Pb runoff to the Labrador Sea

We followed Innocent et al. (1997) and Fagel et al. (1999; 2002, 2004, 2011) in using the mean and median of available whole-rock Pb isotope data to define regional source end-members of Pb runoff from North American and Greenland to the Labrador Sea. We used this approach because we want to compare authigenic Pb isotope data from U1302/3 to estimates of the average weathering signal of regional sources. The mean and median are two ways of estimating this average and the degree of disparity or agreement between them can be used as a first-order-estimate of uncertainty in our understanding of each end-member's average Pb isotope composition (Fagel et al., 2002). Our update to the Fagel et al. (2002) whole-rock Pb isotope compilation (Table 1) refines, however, our understanding of the potential role that changes in Pb provenance may have played in influencing variability in the Pb isotope composition of Orphan Knoll seawater during the LGC.

The heterogenous composition of SP geology reflects its origin as an accretionary orogen composed of many geologically distinct continental and oceanic terranes (Percival, 2007; 2012). The highly radiogenic Pb isotope signal for SP bedrock reported by Fagel et al. (2002) is based on whole-rock records from its southeastern Abitibi Subprovince (Gariepy and Allegre, 1985; Vervoort et al., 1993) - a greenstone-granite belt that has an oceanic-arc origin (Thurston et al., 1991) and is rich in gold and massive sulphide deposits (Mathieu et al., 2020). We lack whole-rock Pb isotope records from most subprovinces of the SP. An examination, though of those that are available for its western and central regions (from the Abitibi, Wawa and Wabigoon subprovinces and Minnesota River Valley terrane) highlights the following: (1) A broad region of the southern SP is on average highly radiogenic ($^{206}Pb/^{204}Pb$ mean = ~22.7; median = ~19.4) in comparison to other North American and Greenland cratonic bedrock, but the SP as a whole is unlikely to be as radiogenic as the Abitibi Greenstone Belt (Fig. 2; $^{206}Pb/^{204}Pb$ mean = ~25.7; median = ~22.7); (2) The average Pb isotope weathering signal of other SP greenstone belts with oceanic-arc affinities (e.g., the western Wabigoon terrane and Wawa Subprovince; see those sectors of the SP highlighted green in Fig. S1) may be as radiogenic as the Abitibi (Table 1; $^{206}Pb/^{204}Pb$ mean = ~29.6; median = ~20.4 and $^{206}Pb/^{204}Pb$ mean = ~21.1; median = ~17.5).

Based on the available evidence, it therefore seems likely that changes in the provenance of Pb runoff could be responsible for at least a portion of the LGM-Holocene radiogenic trend in the Pb isotopic composition of the authigenic Fe–Mn oxyhydroxide fraction of Orphan Knoll sediments. By the same token, it is not clear whether chemical weathering of the Abitibi Greenstone Belt alone could be solely responsible for the most radiogenic early Holocene Pb isotope values reported by Crocket et al. (2012) for our study site. This is because the drainage basins that sample this region of the SP (and host the Nottaway, Harricana, Moose and Albany rivers of Quebec and Ontario) are responsible for only ~22% of modern annual freshwater river discharge to Hudson Bay (Déry et al., 2011)). Yet over 60% of river discharge into Hudson Bay comes from catchment areas that exclusively drain the SP (Déry et al., 2011). It is possible that SP runoff took a different route to the Labrador Sea during the last deglacial. SP runoff into Hudson Bay during T1 would have been restricted by the Hudson Bay Ice Saddle until ~8.1 ka (Dalton et al., 2020). Alternatively, isostatic rebound of North America during T1 could have altered geomorphologic gradients and re-routed SP runoff more directly eastwards into the Labrador Sea. A better appreciation of the magnitude of the role that changes in Pb provenance plays in setting the Pb isotope composition of bottom-waters bathing Orphan Knoll awaits the generation of whole-rock Pb isotope data from a wider region of the SP than is currently available, especially for its greenstone-granite belts with oceanic affinity and similar ore-deposit compositions to the Abitibi Subprovince (see those sectors highlighted green in Fig. S1). In the meanwhile, we discuss the potential role of both Pb provenance and incongruent chemical weathering in driving any radiogenic trends in our datasets.

2.3. Penultimate Glacial Maximum and Last Glacial Cycle ice sheet reconstructions of the Laurentide Ice Sheet

Global sea-level change is a primary indicator of global ice volume and is reasonably well constrained for the past ~130 kyr by data from fossil corals (e.g., Deschamps et al., 2012; Hibbert et al., 2016), submerged speleothems (e.g., Bard et al., 2002; Dorale et al., 2010; Antonioli et al., 2021), planktic foraminiferal $\delta^{18}O$ from restricted basins (e.g., Grant et al., 2014) and benthic foraminiferal $\delta^{18}O$ (e.g., Elderfield et al., 2012), albeit with well-known caveats (e.g., Skinner and Shackleton, 2005; Lisiecki and Raymo, 2009). The history of the individual continental ice-sheets that determines the changes in global sea-level that these records monitor is, however, much less well constrained.

Table 1
Average Pb isotope signature of regional end-members.

Regional source end members	Variable	$^{206}Pb/^{204}Pb$	$^{207}Pb/^{204}Pb$	^{2068} b/^{204}Pb	Data Sources
Superior Province (SP)	Number of data	200			1–9
	Mean	22.724	16.305	42.096	
	Median	19.432	15.780	39.381	
Abitibi Subprovince (SP)	Number of data	55			1–2
(Greenstone Belt)	Mean	25.700	16.999	44.524	
	Median	22.719	16.226	42.831	
Wawa Subprovince (SP)	Number of data	62			3–4
(Greenstone Belt)	Mean	21.132	16.136	40.684	
	Median	17.532	15.572	37.519	
Western Wabigoon terrane (SP)	Number of data	25			5–6
(Greenstone Belt)	Mean	29.576	17.636	48.989	
	Median	20.374	15.842	40.357	
Minnesota River Valley terrane (SP)	Number of data	2			9
	Mean	18.464	15.799	42.165	
	Median	18.464	15.799	42.165	
Churchill Province	Number of data	24			4, 10–11
	Mean	16.495	15.334	36.667	
	Median	16.664	15.303	36.290	
Nain Province	Number of data	49			12–14
	Mean	15.078	14.731	35.517	
	Median	14.697	14.593	35.619	
Grenville	Number of data	185			14–17
	Mean	17.463	15.483	37.526	
	Median	17.433	15.521	37.232	
Ketilidian Mobile Belt	Number of data	76			18–19
	Mean	20.670	15.584	38.765	
	Median	20.252	15.555	38.312	
Archean Block	Number of data	316			19–24
	Mean	14.543	14.475	35.584	
	Median	14.016	14.440	34.527	
Nagssugtoqidian Mobile Belt	Number of data	223			25–28
	Mean	17.220	15.278	38.259	
	Median	16.571	15.260	37.014	
East Caledonides	Number of data	12			29–32
	Mean	17.538	15.314	38.620	
	Median	17.960	15.439	38.630	
Paleogene Volcanics	Number of data	81			33–38
	Mean	17.710	15.331	37.861	
	Median	18.025	15.401	38.010	
North American aeolian dust	Number of data	52			39–40
	Mean	18.865	15.655	38.907	
	Median	18.880	15.655	39.053	

Here, we follow Innocent et al. (1997) and Fagel et al. (1999; 2002, 2004, 2011) in using the mean and median of whole-rock data to define the Pb isotope composition of regional source end-members (see Fig. 2 and Figs. S4-16). This approach provides us with two estimates of the average weathering Pb isotope signal of each source based on the available whole-rock data. The degree of disparity between the mean and the median can be used as a first-order estimate of uncertainty in our understanding of each end-member's average Pb isotope composition. The true average composition for each source likely falls somewhere between these two parameters. Data sources: (1) Gariepy and Allegre (1985); (2) Vervoort et al. (1993); (3) Smith (1988); (4) Thorpe (2008); (5) Wu et al. (2016); (6)Foland (1982); (7) Richardson et al. (2005); (8) Stevenson et al. (1999); (9) Doe and Delevaux (1980); (10) Peterson et al. (1994); (11) Thorpe (1982); (12) Baadsgaard et al. (1979); (13) Schiøtte et al. (1993); (14) Ashwal et al. (1986); (15) Scharer (1991); (16) Arcuri and Dickin (2018); (17) Sinha et al. (1996); (18) Kalsbeek and Taylor (1985); (19) Taylor and Upton (1993); (20) Moorbath et al. (1981); (21) Taylor et al. (1992); (22) Taylor et al. (1984); (23) Taylor et al. (1980); (24) Baadsgaard et al. (1986); (25) Kalsbeek et al. (1984); (26) Kalsbeek et al. (1988); (27) Kalsbeek et al. (1987); (28) Kalsbeek et al. (1993); (29) Hansen and Friderichsen (1989); (30) Thrane (2004); (31) Jensen (1994); (32) Ellam and Stuart (2000); (33) Andreasen et al. (2004); (34) Barker et al. (2006); (35) Hansen and Nielsen (1999); (36) Farmer et al. (2003); (37) Saunders et al. (1999); (38) Holm (1988); (39) Jardine et al. (2021); (40) Aleinikoff et al. (2009).

The LIS was the largest continental ice-sheet in the northern hemisphere at the LGM. Its spatial extent at that time is widely documented by glaciomorphological evidence (e.g., Dyke et al., 2002) and inverse modelling (e.g., Lambeck et al., 2014). Our understanding of the evolution of its spatial extent prior to the LGM is, nevertheless, rudimentary (Ehlers et al., 2011). In this study, we focus on reconstructing LIS history prior to the LGM and as far back as MIS 6. Limited terrestrial glaciomorphological evidence exists for LIS extent for this time because any evidence would likely have been destroyed during its Last Glacial advance and what remains is challenging to date. Instead, most inferences of LIS evolution prior to the LGM are based on numerical models underpinned, where available, by scant empirical data (e.g., Colleoni et al., 2016; Stokes et al., 2012). This combined approach forms the basis of a recent synthesis by Batchelor et al. (2019) that arguably provides our current best constraints on pre-LGM ice sheet configurations in terms of a 'minimum', 'maximum' and 'best-estimate' for LIS extents for all isotope stages. Here we test these estimates for the past ~130 kyr, alongside insights provided by selected subsequently published research (e.g., Dalton et al., 2019; Kerr et al., 2021) using our new Pb isotope data (Figs. 3 and 4). We focus on reconstructing chemical weathering and runoff flux of North American bedrock adjacent to Hudson Bay because they underly a key sector of the LIS that is home to the biggest ice-stream of the Last Glacial (the Hudson Bay Ice Stream) and freshwater runoff from these landmasses represents the dominant source today of dissolved Pb that is ultimately routed to our study site via the Labrador Current.

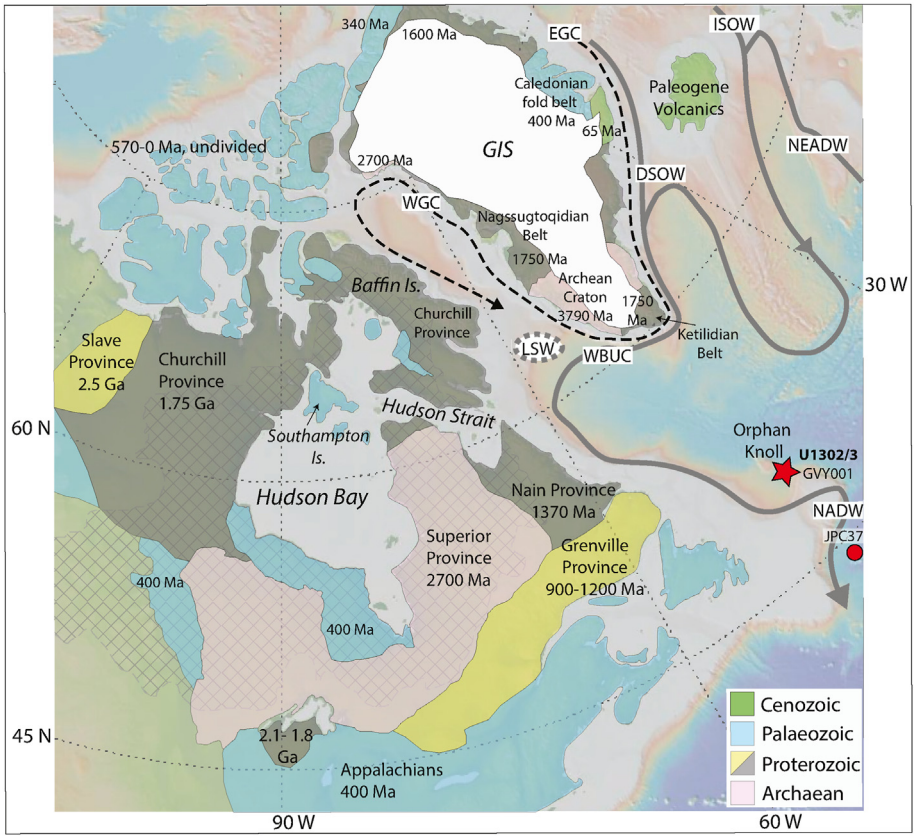

Fig. 1. Map showing location of IODP Site U1302/3 and other sites discussed in the text, and relevant surrounding cratonic (bedrock) geology. Geology of North America and Greenland redrawn from Reed et al. (2005) and White et al. (2016). Grey hatched region denotes modern area of watershed drainage into Hudson Bay and its straits (Natural Resources Canada, 2006). Arrows denote paths of key modern deep (solid grey) and surface (dashed grey) ocean currents relevant to this study (redrawn from Blake-Mizen et al., 2019). GIS = Greenland Ice Sheet. ISOW = Iceland-Scotland Overflow Water. DSOW = Denmark-Scotland Overflow Water. NEADW = Northeast Atlantic Deep Water. WBUC = Western Boundary Undercurrent. LC = Labrador Current. LSW = Labrador Sea Water. NADW = North Atlantic Deep Water. WGC = West Greenland Current. EGC = East Greenland Current.

3. Methods

3.1. Site description, sampling and age model

IODP Site U1302 (50° 10′N, 45° 38.3′W, water depth: 3560 m) and Site U1303 (50° 12.4′N, 45°41.2′W, water depth: 3520 m) are located on the SE flank of Orphan Knoll within the Labrador Sea, proximal to the coast of Newfoundland (Channell et al., 2006). They are positioned on a rise between two canyons that help to protect these sites from debrite and turbidite deposition by funnelling gravity flows down slope (Aksu and Hiscott, 1992). They are only ~3 nautical miles apart and have remarkably similar sedimentology (Expedition 303 Scientists et al., 2006). The similarity of strata between the two sites permitted the creation of a continuously spliced composite record using both sites based on correlation of physical property data down to 104 m composite depth (mcd; Expedition 303 Scientists et al., 2006).

To extend the previously published record of the Pb isotopic composition of the Fe–Mn oxyhydroxide fraction of sediments deposited at Site U1302/3 spanning the last ~37 kyr (Crocket et al., 2012) back to ~130 ka (MIS 3–6), 5-cc samples were taken every 10–50 cm (83 in total) between 0.45 and 23.38 mcd. The same samples were also used to determine the elemental concentrations of the seawater derived Fe–Mn oxyhydroxide fraction. A subset of these samples (n = 18) were used to determine the Pb isotope composition and elemental composition of the detrital fraction. A further four samples were taken between 0.45 and 4.71 mcd to evaluate the reproducibility of our new data with those reported by Crocket et al. (2012). Highly radiogenic Pb isotope excursions in authigenic Fe–Mn oxyhydroxide data derived from detrital carbonate (Heinrich) layers deposited at Site U1302/3 are suggested to represent exceptionally high inputs of detrital particles containing a "pre-formed" coating sourced from Hudson Bay during destabilisation of the LIS (Crocket et al., 2012). Not all past episodes of enhanced detrital inputs to the Labrador Sea are expressed in the Site U1302/3 stratigraphy by clear sedimentological layers. Because we are only interested in the evolution of seawater Pb isotope compositions in the Labrador Sea over the past ~130 kyr, we therefore used the XRF-derived detrital-layer stratigraphy for Site U1302/3 (Channell et al., 2012) to minimise sampling the pre-formed signal of the detrital carbonate layers.

The age model for our record was generated by Channell et al. (2012), based on matching relative palaeointensity (RPI) and $\delta^{18}O$ data from *Neogloboquadrina pachyderma* (*sin.*) to the PSIO-1500 RPI stack (Channell et al., 2009) and the LR04 benthic $\delta^{18}O$ stack (Lisiecki and Raymo, 2005). The detrital layer stratigraphy for our study site (Channell et al., 2012) also permits confident correlation of our datasets to those of other North Atlantic marine cores where Heinrich event iceberg rafting events have been identified.

3.2. Pb isotope analysis

All sample processing and laboratory analyses were conducted at the School of Ocean and Earth Science, University of

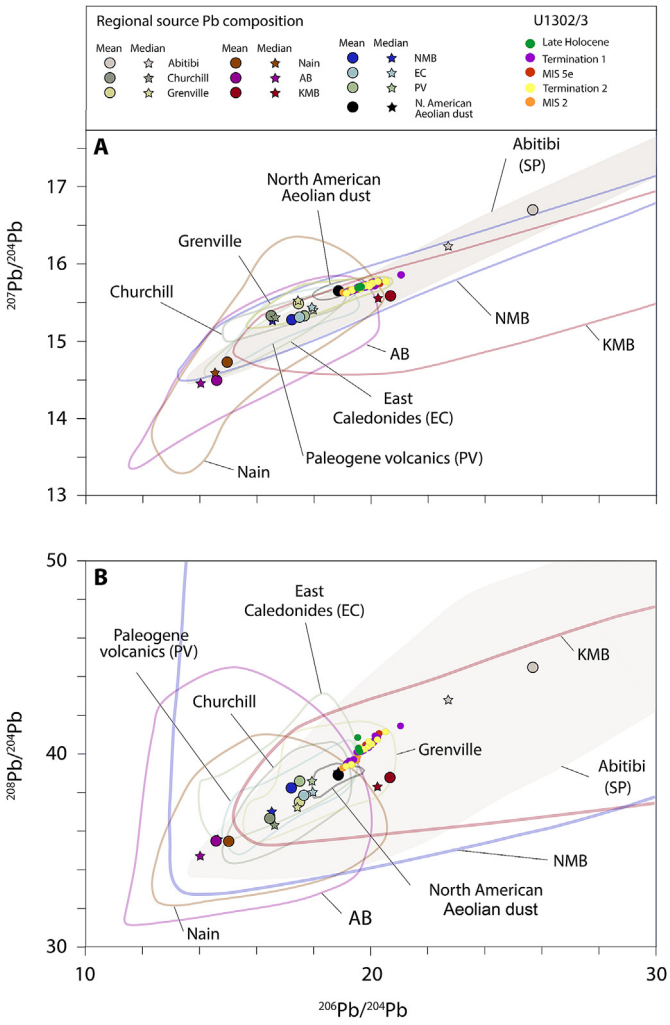

Fig. 2. The Pb isotope composition of cratonic bedrock adjacent to Orphan Knoll Site U1302/3: **(A)** $^{206}Pb/^{204}Pb$ versus $^{207}Pb/^{204}Pb$ and **(B)** $^{206}Pb/^{204}Pb$ versus $^{207}Pb/^{204}Pb$. Based on a whole rock data compilation by Fagel et al. (2002), supplemented by additional datasets (see Table 1, Figs S4-16). The Pb isotopic composition of the authigenic Fe–Mn oxyhydroxide fraction of U1302/3 sediments is also shown for the late Holocene (green circles), Termination 1 (purple circles), MIS 3 (blue circles), MIS 5d-a (red circles), Termination 2 (yellow circles) and MIS 4, 2 (orange circles). See Fig. 1 for craton locations. We defined the average weathering Pb isotope signal of each source following Innocent et al. (1997) and Fagel et al. (1999; 2002, 2004, 2011) by using the mean and median of the whole-rock data available for each craton. The degree of disparity between the mean and the median can be used as a first-order estimate of uncertainty in our understanding of each end-member's average Pb isotope composition. (For interpretation of the references to colour in this figure legend, the reader is referred to the Web version of this article.)

Southampton. We extracted Pb from the authigenic Fe–Mn oxyhydroxide fraction in sediments of each sample closely following Blaser et al. (2016). Briefly, between 25 and 30 mg of dried, homogenised sediment was washed with ultra-pure water (18.2 MΩ) for 20 min on a vertical tube rotator, centrifuged at 3200 rpm for 7 min and decanted. The samples were then exposed to a leaching solution to extract only the seawater derived Fe–Mn oxyhydroxide fraction of sediment. The leaching solution (hereafter HH-leach) was a mixture of 3 mM Na-EDTA, 5 mM hydroxylamine-hydrochloride, 1.5% acetic acid and buffered to pH 4 using 0.04 M NaOH. Following addition of 10 ml HH-leach, samples were resuspended using a vortex mixer, degassed to release any carbon dioxide from carbonate dissolution and placed on a vertical tube rotator for 20 min to ensure all sediment was exposed to the reductive complexing solution. Samples were further centrifuged at 3200 rpm for 7 min and the solution pipetted into vials and prepared for analysis.

To ensure 200 ng of Pb was obtained for column chemistry, an aliquot of each leached solution was screened on a Thermo Scientific X-Series 2 ICP-MS. Based on the Pb concentration obtained through the above screening, an aliquot of leached solution was evaporated to dryness in Teflon pots, followed by the addition of 0.5 ml concentrated HNO_3 and left overnight on a hot plate at 130 °C to react. The samples were left to evaporate to dryness followed by the addition of 0.5 ml 0.5 M HBr and left on a hotplate at 130 °C for at least 1 h. The Pb fraction was separated from the matrix using Eichrom AG1-X8 200–400 mesh anion exchange resin (Strelow, 1978). The resultant aliquots were screened on a Thermo Scientific X-Series 2 ICP-MS to measure the Pb concentration to allow accurate spiking for isotope analysis.

To confirm that the above procedure was successful at extracting a seawater Pb signal, 30 of the same samples spanning the record were analysed for detrital (residual fraction) Pb isotopes. Samples were exposed to a second HH-leach with 10 × solution strength for 24 h on a vertical tube rotator to ensure complete removal of Fe–Mn oxyhydroxides following Gutjahr et al. (2007). The samples were then centrifuged, decanted, washed in Milli-Q water and decanted again. After drying, 100 mg of homogenised sediment was weighed into Teflon pots and subject to 3 ml aqua regia overnight to remove organic compounds, evaporated to dryness and redissolved in concentrated HNO_3. The remaining silicates were digested in 2 ml of HF for 48 h at 130 °C. Finally, $HClO_4$ was added and left overnight at 130 °C. Once dried, a few drops of 6 M HCl were added for 24 h at 130 °C, dried and repeated. Stock solutions were comprised of the sample, ~10 ml 6 M HCl and Milli-Q. These detrital fraction solutions were prepared for column chemistry following the same procedure as outlined above for the Fe–Mn oxyhydroxide fraction solutions.

Pb isotope ratios were measured using a Thermo Neptune MC-ICP-MS, after the samples were diluted with 3% HNO_3 to obtain ~20 ng/ml of Pb. A double spike run for each sample was used to correct for instrumental mass fractionation where the ^{207}Pb–^{204}Pb SBL74 spike (Taylor et al., 2015) was added such that $^{204}Pb_{sample}/^{204}Pb_{spike}$ was 0.09 ± 0.03. Procedural blanks for Fe–Mn oxyhydroxide and detrital fraction samples averaged 0.028 ng (n = 14) and 0.001 ng Pb (n = 1), respectively with samples being blank-corrected. Blanks were treated in the same way as sediment samples to determine possible contamination from reagents and general handling. Authigenic Pb masses range from ~36 to 198 ng. Reproducibility of Pb isotope ratios was estimated based on 17 measurements of the standard SRM NBS 981 run from 2018 to 2020. This analytical period yielded average ratios and uncertainties at 2σ (relative to the values of Baker et al. (2004) as shown in parentheses): $^{206}Pb/^{204}Pb$ = 16.9424 ± 0.00044 (16.942 ± 0.00006), $^{207}Pb/^{204}Pb$ = 15.4982 ± 0.00097 (15.501 ± 0.00006) and $^{208}Pb/^{204}Pb$ = 36.7182 ± 0.00276 (36.730 ± 0.00019). All accuracies are <1%. To monitor reproducibility of Pb isotope ratios further, an internal replicate of an authigenic Fe–Mn oxyhydroxide sample from IODP Site U1302/3 was measured in every run (n = 5), producing average ratios of $^{206}Pb/^{204}Pb$ = 19.1946 ± 0.000416 (2σ; variance = 0.0057 ± 0.0008), $^{207}Pb/^{204}Pb$ = 15.6341 ± 0.000859 (2σ; variance = 0.0042 ± 0.0001) and $^{208}Pb/^{204}Pb$ = 3.5237 ± 0.00205 (2σ; variance = 0.000071 ± 0.0008).

3.3. Rare and trace elements analysis

Trace element concentrations of the Fe–Mn oxyhydroxide

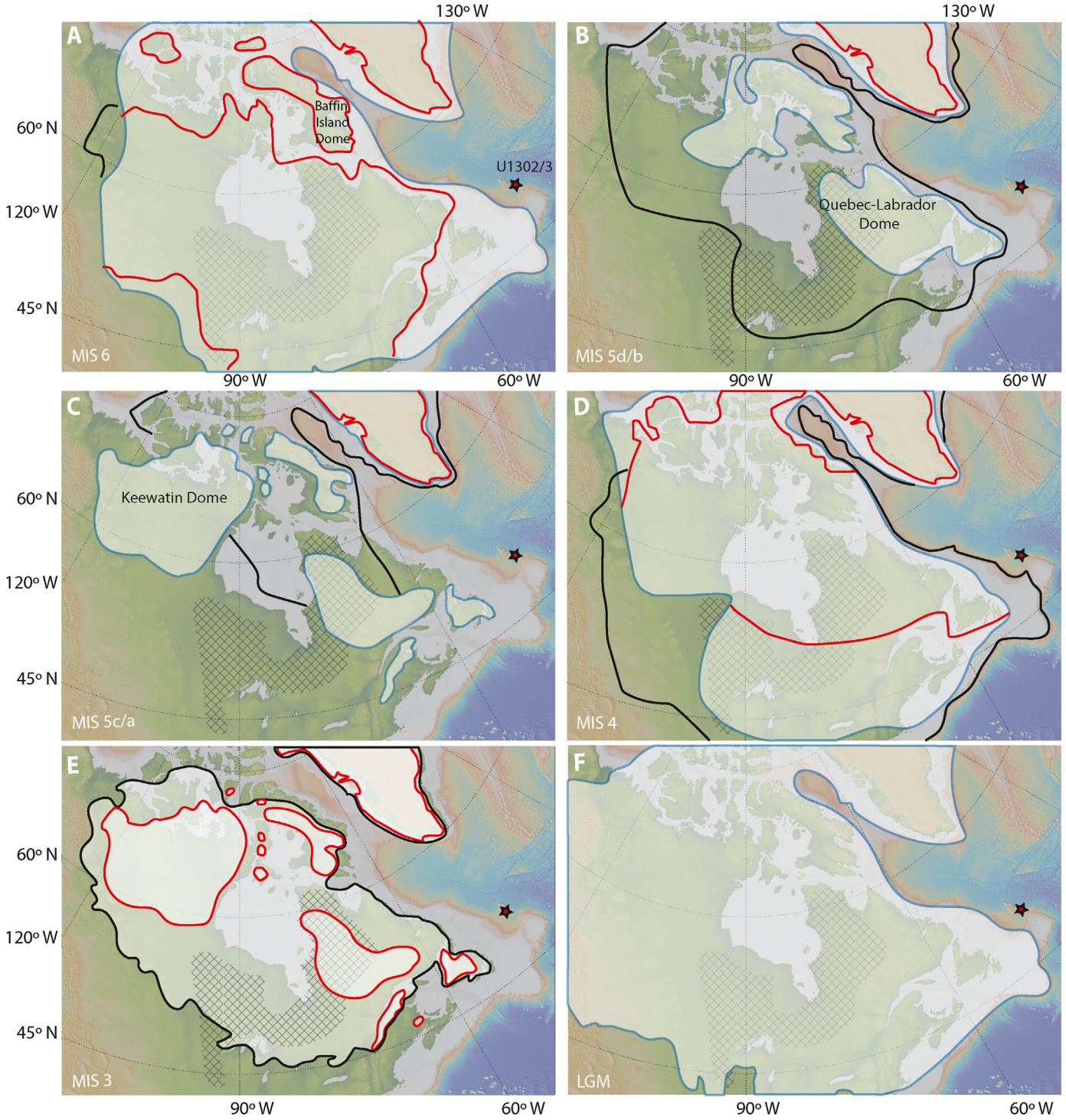

Fig. 3. Reconstructions of Laurentide Ice Sheet and Greenland Ice Sheet extents following Batchelor et al. (2019). Maximum (black line), minimum (red line) and best-estimate (blue) ice-sheet extents for: **(A)** marine isotope stage (MIS) 6 (132–140 ka); **(B)** MIS 5d/b (108–117; 86–92 ka, respectively); **(C)** MIS5c/a (92–108; 72–86 ka); **(D)** MIS 4 (58–72 ka); **(E)** MIS 3 (29–57 ka) where minimum estimate is at peak warmth (40–45 ka; red line) and maximum estimate achieved following a period of LIS growth (30 ka; black line); **(F)** Last Glacial Maximum (26–19 ka). Black cross-hatched area denotes geographical extent of Superior Province craton (Montsion et al., 2018). Red stars highlight location of IODP Site U1302/3 on Orphan Knoll. (For interpretation of the references to colour in this figure legend, the reader is referred to the Web version of this article.)

fraction stock solutions were also used to evaluate the fidelity of our seawater Pb isotope data. To generate these data, 100 μl aliquots of the above mentioned stock solutions were dried in Teflon pots, then concentrated HNO_3 was added to remove HH-leach chemicals. The samples were dried and dissolved in 3% HNO_3 spiked with In (5 ppb), Re (5 ppb) and Be (20 ppb) to achieve a 100 × dilution. Analyses were conducted on the Thermo Scientific X-Series 2 ICP-MS. Measurements were calibrated using a suite of international rock standards; JB-1a, JGB-1, BIR-1, BHVO-2, JB-3, JB-2, BCR-2, AGV-2 that were diluted with 3% HNO_3 spiked with In (5 ppb), Re (5 ppb) and Be (20 ppb) to achieve an ~4000 × dilution for the trace elements. An additional set of standards were run with

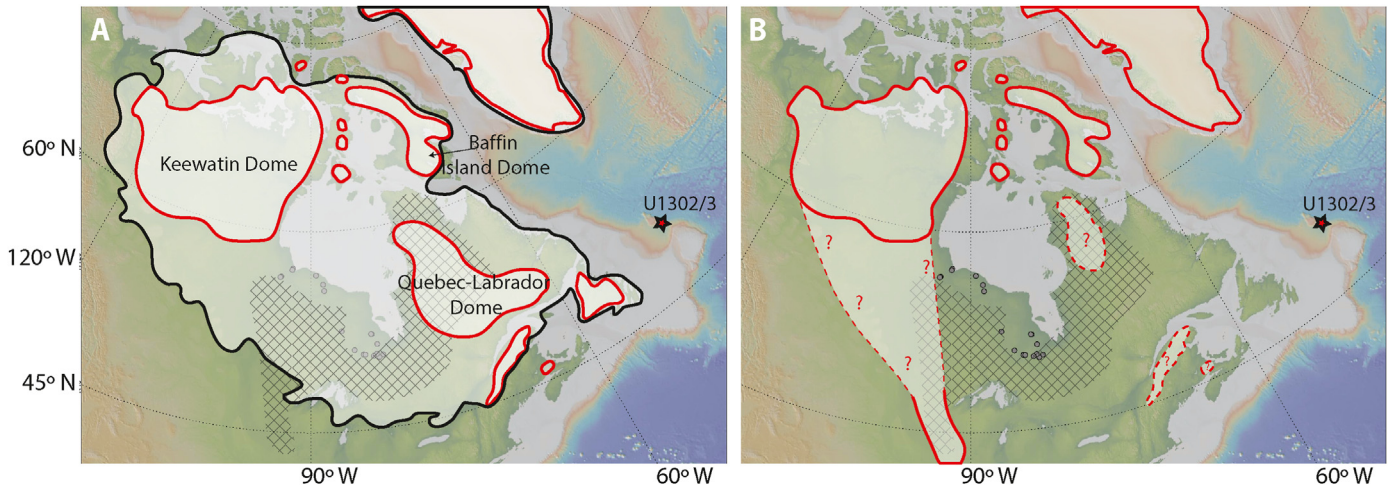

Fig. 4. Reconstructions of Northern Hemisphere ice-sheet extents for marine isotope stage (MIS) 3 (29–57 ka): **(A)** following Batchelor et al. (2019) where minimum estimate shown in (A) (red line) is at peak warmth (40–45 ka) and maximum estimate shown (black line) is during a subsequent period of LIS growth (30 ka)**; (B)** peak warmth (40–45 ka) following Pico et al. (2017), Dalton et al. (2019) and Kerr et al. (2021) where dashed red line is inferred ice extent. Black cross-hatched area denotes geographical extent of Superior Province (Montsion et al., 2018). Grey circles (n = 35) represent locations of ^{14}C and optically stimulated luminescence geochronological dates of marine and fluvial strata from the Hudson Bay Lowlands used by Dalton et al. (2016, 2017; 2019) to infer a marine incursion into this area (and its deglaciation) between 52–42 ka. (For interpretation of the references to colour in this figure legend, the reader is referred to the Web version of this article.)

~80,000 × dilution for Al and Fe. In-house reference materials BAS206 and BRR-1 and international reference material JA-2 were also run after the standards. Long term accuracy of JA-2 relative to the reference value (Jochum et al., 2016) is better than 5% except for Cu and Pb which are 6% and 7%, respectively.

Rare earth element (REE) concentrations of the samples were expressed relative to the REE profile of the Post-Archean Australian Shale (PAAS), which is a good approximation of the upper continental crust (Taylor and McLennan, 1985). To characterise REE patterns, ratios of PAAS-normalised concentrations were used following Martin et al. (2010) and Blaser et al. (2016, 2019) and shown in Eqs. (1)–(6):

$$\text{Light REE:} \quad LREE = La_n + Pr_n + Nd_n \tag{1}$$

$$\text{Heavy REE:} \quad HREE = Er_n + Yb_n + Lu_n \tag{2}$$

$$\text{Middle REE:} \quad MREE = Gd_n + Tb_n + Dy_n \tag{3}$$

$$\text{REE slope:} \quad HREE / LREE \tag{4}$$

$$\text{REE bulge:} \quad MREE/MREE^* = MREE/0.5(HREE + LREE) \tag{5}$$

$$\text{where} \quad REE_n = = REE_{sample} \Big/ REE_{PAAS} \tag{6}$$

4. Results and discussion

4.1. New LGC Pb isotope data from site U1302/3

In Fig. 5 we integrate our new and published data to present the first high resolution LGC records of authigenic Fe–Mn oxyhydroxide-derived Pb isotopes from the subpolar North Atlantic that spans both the last (T1) and penultimate (T2) deglaciations. Comparable values, where overlap exists (for the LGM to Holocene), between our new data from Orphan Knoll Site U1302/3 and those previously published by Crocket et al. (2012) for this site, confirm the validity of splicing these two records together (see overlap of filled and white circles between 37 and 0 ka in Fig. 5c–e).

The new longer record from Site U1302/3 confirms the suggestion of Crocket et al. (2012) that the U1302/3 authigenic signal of sediments deposited at our study site is characterised by short-lived highly radiogenic excursions during the deposition of Heinrich-like layers in the Labrador Sea (see Pb data within green and light yellow vertical bars in Fig. 5c–e). However, on orbital timescales, Pb isotope ratios typically vary between ~19 and 21.5 ($^{206}Pb/^{204}Pb$), ~15.6 to 16 ($^{207}Pb/^{204}Pb$) and ~40.5 to 42 ($^{208}Pb/^{204}Pb$) with relatively radiogenic values occurring during warm stages MIS 5, 3 and 1, and the least radiogenic values occurring during cold stages MIS 6, 4 and 2 (Fig. 5c–e). While only the oldest datapoints in our Pb isotope records capture MIS 6, they suggest that the Pb isotope composition of seawater bathing U1302/3 during this time was likely just as unradiogenic as during MIS 4 and 2 (Fig. 5c–e). The magnitude of change in Pb isotope ratios across T2 is comparable to its evolution across T1 (compare Pb isotope zones β & γ to θ & ι in Fig. 5c–e), but this pattern of change occurs more rapidly across T2 (~7 kyr) vs. T1 (~17 kyr). Strikingly, from MIS 5d to 5a, ratios become progressively more radiogenic (from ~19.5–21.7 for $^{206}Pb/^{204}Pb$; Pb isotope zone δ in Fig. 5c–e; also see Fig. S2). LGM-like values are first recorded during the LGC in MIS 4 (Pb isotope zone ε in Fig. 5c–e) but return to ratios closest to late Holocene compositions (~19.6 $^{206}Pb/^{204}Pb$) during MIS 3 (Pb isotope zone ζ in Fig. 5c–e). By contrast, the detrital fraction Pb isotope record shows different absolute ratios (e.g., ~16–18 for $^{206}Pb/^{204}Pb$) and contrasting temporal trends to that recorded by the authigenic records (compare Fig. 5c–e to 5fh; also see Fig. S3).

4.2. Fidelity of the authigenic Fe–Mn signal from Site U1302/3 as a record of Labrador Sea seawater Pb isotope composition

To assess the integrity of the seawater Pb isotope record extracted from the authigenic Fe–Mn oxyhydroxide sediment fraction, we employ a series of tests to check for the possible release of non-seawater-derived Pb from the detrital sediment fraction. These tests are: (1) examination of detrital and authigenic Pb isotope trends for evidence of covariance, (2) evaluation of REE data to identify what material was leached (Haley et al., 2004; Martin

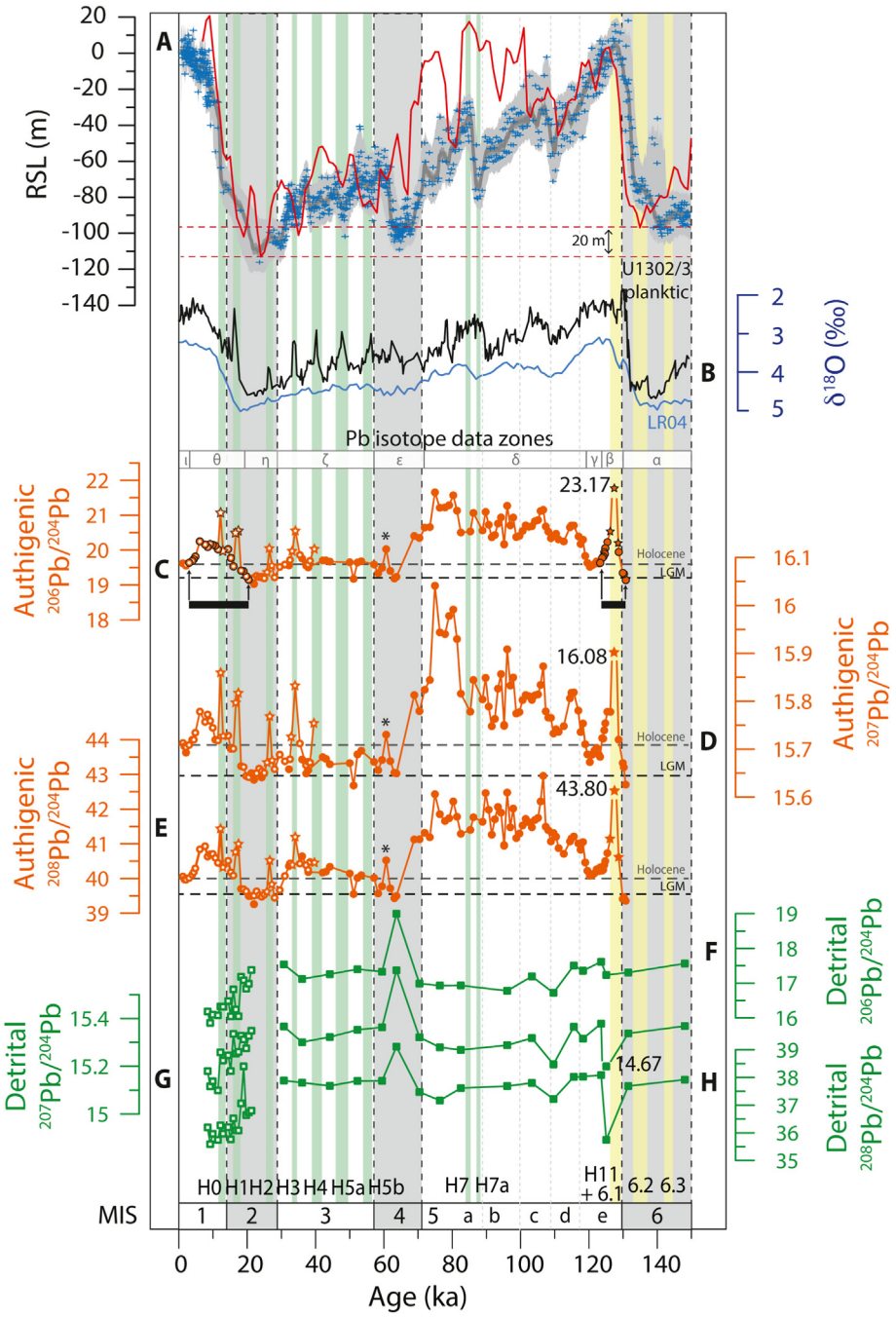

Fig. 5. Pb isotope and $\delta^{18}O$ records from IODP Site U1302/3 spanning marine isotope stage (MIS) 6–1: **(A)** Relative sea-level (RSL) record from the Red Sea with data points (blue crosses), 95% probability interval for the RSL data (dark grey envelope) and 95% probability interval for the probability maximum (light grey envelope; Grant et al., 2012). Also shown is a benthic foraminiferal-derived RSL record from Ocean Drilling Program Site 1123 (red line; Elderfield et al. (2012)) and the PGM-LGM difference in global sea-level (horizontal dashed lines); **(B)** U1302/3 planktic $\delta^{18}O$ (black line; Hillaire-Marcel et al., 2011) and the LR04 benthic $\delta^{18}O$ stack (blue line; Lisiecki and Raymo, 2005); Pb isotope ratios of authigenic Fe–Mn oxyhydroxides: **(C)** $^{206}Pb/^{204}Pb$; **(D)** $^{207}Pb/^{204}Pb$; **(E)** $^{208}Pb/^{204}Pb$; Pb isotope ratios of detrital sediment fraction: **(F)** $^{206}Pb/^{204}Pb$; **(G)** $^{207}Pb/^{204}Pb$; **(H)** $^{208}Pb/^{204}Pb$ ratios of Site U1302/3. "Detrital" refers to the full digestion of the authigenic-free fraction of marine sediment. Solid circles/stars = this study; open circle/stars = Crocket et al. (2012). MIS cold (warm) stages are shown by vertical light grey (white) bars. Heinrich (detrital) layers preserved in both the Labrador Sea (identified using core-scanning-derived XRF Ca/Sr ratios by Channell et al. (2012)) and subpolar North Atlantic sediments (Hemming, 2004; Hodell et al., 2008) are shown by labelled vertical light green bars. Labelled vertical light-yellow bars highlight Heinrich-like detrital layers where deposition was restricted to the Labrador Sea (Channell et al., 2012; Hodell et al., 2008). Star-shaped symbols denote Pb isotope data from U1302/3 detrital layers. Horizontal dashed lines in (C) (D) and (E) highlight Pb isotopes values at U1302/3 during the late Holocene and Last Glacial Maximum. Horizontal black bars and arrows in (C) highlight intervals over which we infer enhanced supply of dissolved radiogenic weathered material from the Superior Province craton exposed following Laurentide Ice Sheet retreat in the Hudson Bay region during Terminations 2 and 1 (data symbols in CE with black outlines). Greek symbols α-ι labelled in (C) correspond to Pb isotope data zones referred to in main text. See Fig. 1 for site locations. (For interpretation of the references to colour in this figure legend, the reader is referred to the Web version of this article.)

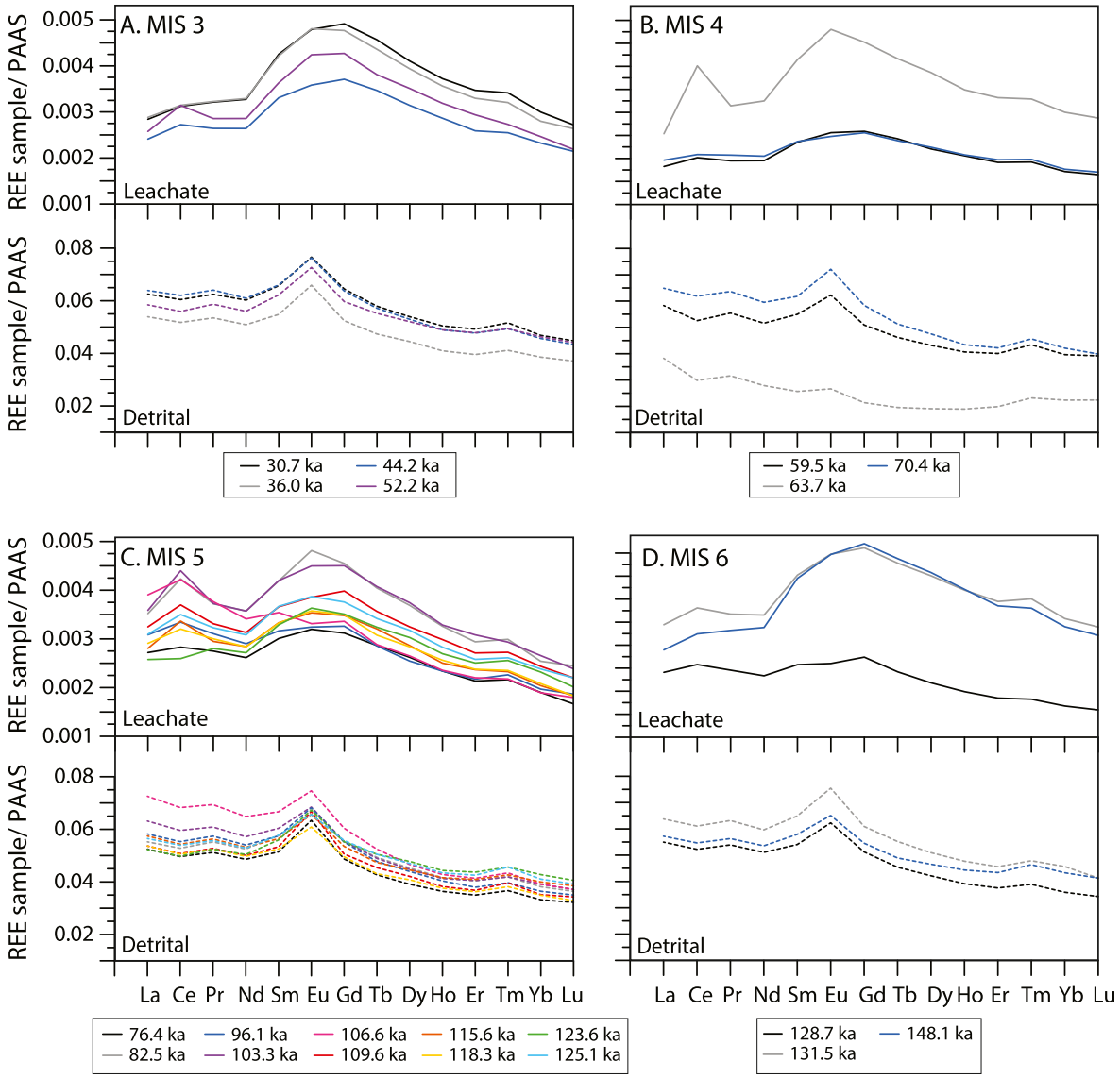

Fig. 6. Post-Archean Australian shale (PAAS) normalised rare earth element (REE) multi-element plots for paired authigenic Fe–Mn oxyhydroxide (solid lines) and detrital (dotted lines) samples deposited at IODP Site U1302/03 during (A) marine isotope stage (MIS) 3, **(B)** MIS 4, **(C)** MIS and **(D)** MIS 6.

et al., 2010) and, (3) comparison of Al/Nd, Al/Pb and Al/Th ratios of the authigenic and detrital fractions of our samples and abyssal ocean Fe–Mn crusts (Gutjahr et al., 2007).

The absence of any significant covariance between trends in the authigenic and detrital Pb isotope records (compare panels c–e to fh in Fig. 5; Fig. S3) strongly suggests that detrital sediment leaching during sample processing does not control temporal variability in our leachate record. This is confirmed by the presence of a distinct PAAS-normalised mid-REE (MREE) enrichment in our leachate samples that is not characteristic of the distribution of REE in our detrital samples (Fig. 6; Piper, 1974). This MREE enrichment is somewhat different from water column REE concentration patterns (e.g. Patton et al., 2021) and considered characteristic of marine pore waters because particulate Fe^{3+} oxides are reduced and dissolved in pore waters to release REE scavenged in the water column (Haley et al., 2004). It has been shown that the REE signature of HH-extracted leachate seawater signals plots separately from that of the residual detrital fraction in cross plots of the REE slope (HREE/LREE) and MREE bulge (MREE/MREE*) (Haley et al., 2004; Martin et al., 2010). Most of the samples analysed in this study plot in this region (Fig. 7). Yet some of our MIS 5 authigenic data (n = 18 out of 83) encroach on the detrital field (red and yellow triangles in Fig. 7a–b) consistent with incomplete removal of oxides, partial leaching of the detrital component during sediment processing (Martin et al., 2010) or potentially by pore waters in the sediment pile (i.e., in situ chemical weathering at the seafloor after deposition; Blaser et al., 2020). The presence of positive Ce anomalies in some MIS 5 authigenic data may record contributions of detritally-sourced Ce to the leachate signal (Fig. 6). It may also reflect highly elevated early-deglacial trace metal input into the Labrador Sea due to generally highly elevated chemical weathering rates following the LGM (compare with Vance et al., 2009).

These MIS 5 data are characterised by some of the most radiogenic Pb isotope values in our records (of ~21.5 $^{206}Pb/^{204}Pb$; Fig. 5c–e). The general absence of detrital H-layer deposition at U1302/3 during this interval (green/light yellow bars in Fig. 5) rules out leaching of preformed radiogenic coatings from sediments sourced from Hudson Bay for the origin of this signal (Crocket et al.,

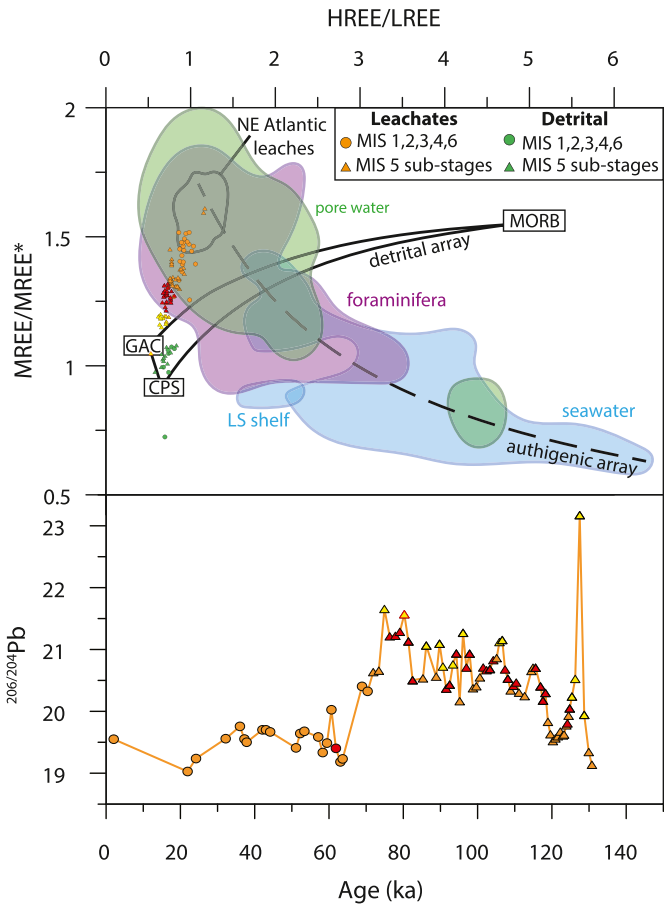

Fig. 7. Comparison of PAAS normalised rare earth element (REE) slope (HREE/LREE) and mid-REE bulge (MREE/MREE*) of detrital sediment samples and their authigenic Fe–Mn oxyhydroxides coatings deposited at IODP Site U1302/3 during marine isotope stages (MIS) 6–1 (0–145 ka). Corresponding $^{206}Pb/^{204}Pb$ ratios are shown in the bottom panel. Seawater, pore fluids, foraminifera and authigenic phase fields shown are from Blaser et al. (2020): defined using foraminiferal REE data from core top to Last Glacial Caribbean, Northwest Atlantic and Equatorial Pacific sediments (purple, Osborne et al., 2017), seawater data from the eastern subpolar North Atlantic (Crocket et al., 2018), equatorial Atlantic (Zheng et al., 2016), and the Atlantic sector of the Southern Ocean (Hathorne et al., 2015), all blue), and pore water data of three sites from the Oregon margin (green, Abbott et al., 2015b). Northeast Atlantic leaches comprise Holocene and LGM data from Blaser et al. (2019), generated with the same leach method used in this study. The curved dashed line defines a potential "authigenic array" following Du et al. (2016). It is defined by mixing of the most HREE enriched seawater included with the most MREE enriched diagenetic ferromanganese Nodule reported by Bau et al. (2014) from Pacific Ocean Clarion-Clipperton Fracture Zone. The solid black curved lines define a detrital mixing array between Mid Ocean Ridge Basalts (MORB; Gale et al., 2013), Greenland Archean Crust (GAC; Wedepohl et al., 1991), and Canadian Precambrian shield cratonic rocks (CPS; Shaw et al., 1986) following Blaser et al. (2020). (For interpretation of the references to colour in this figure legend, the reader is referred to the Web version of this article.)

2012). We cannot rule out the possibility that the detrital fraction itself was partially leached during the processing of our MIS 5 samples but consider it unlikely (see below). The relatively low MREE/MREE* ratios for many of these samples also suggest in-situ chemical weathering of sediments (i.e., they encroach on the detrital field; see red and yellow triangles in Fig. 7a–b & 8b). Blaser et al. (2020) observed that the Nd isotope composition of the authigenic fraction of U1302/3 sediments can be modified by sediment leaching in pore waters at times of enhanced supply of glacially-eroded materials from Hudson Bay to the Labrador Sea. While sand-sized IRD deposition on Orphan Knoll is negligible during MIS 5 (Fig. 8d–e), XRF-scanning-derived Ca/Sr-ratios, indicative of Hudson Bay-sourced mud, are regularly high throughout MIS 5 (Fig. 8a). While we cannot rule out that in-situ weathering of seafloor sediments occurred at our study site during this time, we contend that the $^{206}Pb/^{204}Pb$ values of ~20.5–21.5 that characterise it must reflect that the Pb isotope composition of seawater bathing our study site during MIS 5d-a was unusually radiogenic in the context of the past ~130 kyr. This is because the Pb isotope composition of the detrital fraction deposited at U1302/3 during MIS 5 is much more unradiogenic than the authigenic signal (by ~3–4 units), so its partial leaching through in-situ weathering would make seawater and authigenic Pb isotope compositions more unradiogenic. In-situ weathering would therefore act to mask a radiogenic seawater signal, not artificially imprint one. Given that Pb is much more particle-reactive than most REE, we also note that partial release of terrigenous REE during in-situ weathering at the seafloor does not necessarily result in the release of comparable quantities of Pb (Henderson and Maier-Reimer, 2002).

The IRD records from Orphan Knoll leave open the possibility that the onset of LGM-like unradiogenic authigenic Pb isotope ratios in our new data during MIS 4 was influenced by in-situ porewater leaching of old (unradiogenic) cratonic materials delivered to our study site via iceberg rafting (Fig. 8d–e). While we cannot rule out that in-situ chemical weathering of IRD influenced the Pb isotope composition of seawater bathing our study site to some extent during the Last Glacial, we consider it unlikely that it is responsible for the major trends in our records. The highest deposition rates (and sediment concentrations) of IRD on Orphan Knoll occurred during MIS 2 (Fig. 8d–e; Zhou et al., 2021), meaning that if in-situ chemical weathering of IRD controlled the trends in our authigenic Pb isotope records the values we observe for MIS 4 should be more radiogenic than those reported for the LGM, but they are not (Fig. 8c). In any case, the Al/Nd, Al/Th and Al/Pb ratio compositions of the authigenic fraction for all our samples are closest to those of deep ocean Fe–Mn crusts that represent a pristine seawater signal and are significantly lower than the Al/Nd, Al/Th and Al/Pb ratios of their detrital counterparts (Fig. 9). We therefore conclude that the major trends in U1302/3 authigenic Pb isotope data are not dominated by release of Pb from sediments deposited in the Labrador Sea during the LGC.

4.3. *What does the evolution of authigenic Pb isotopes at U1302/3 reveal about Laurentide Ice Sheet extent over the past ~130 kyr?*

An increase in (i) physicochemical weathering intensity, (ii) incongruent weathering of highly reactive weakly-chemically altered glacial debris on North America (Crocket et al., 2012) and (iii) enhanced sourcing of weakly-weathered SP radiogenic material (Blaser et al., 2020) have been proposed to explain how the Pb isotope composition of bottom waters bathing U1302/3 can become more radiogenic following LIS retreat. Regardless of which of these mechanism prevail, our new Pb isotope records from U1302/3 provide a way to shed new light on the evolution of the spatial extent of the LIS back to T2.

4.3.1. *MIS 6 and Termination 2 LIS history*

The Batchelor et al. (2019) reconstruction for MIS 6 suggests Hudson Bay was glaciated throughout the PGM, but no accurately dated empirical data exist that can be used to ground-truth this suggestion. While only the oldest datapoints in our Pb isotope records were recovered from the end of MIS 6 according to our RPI-based age model, they suggest that the Pb isotope composition of seawater bathing U1302/3 just prior to Termination 2 were just as unradiogenic as during the LGM at this site (compare Pb isotope zones α & η in Fig. 5c–e; Fig, 10). Our new data therefore suggest that the spatial footprint of the LIS in Hudson Bay and the degree to

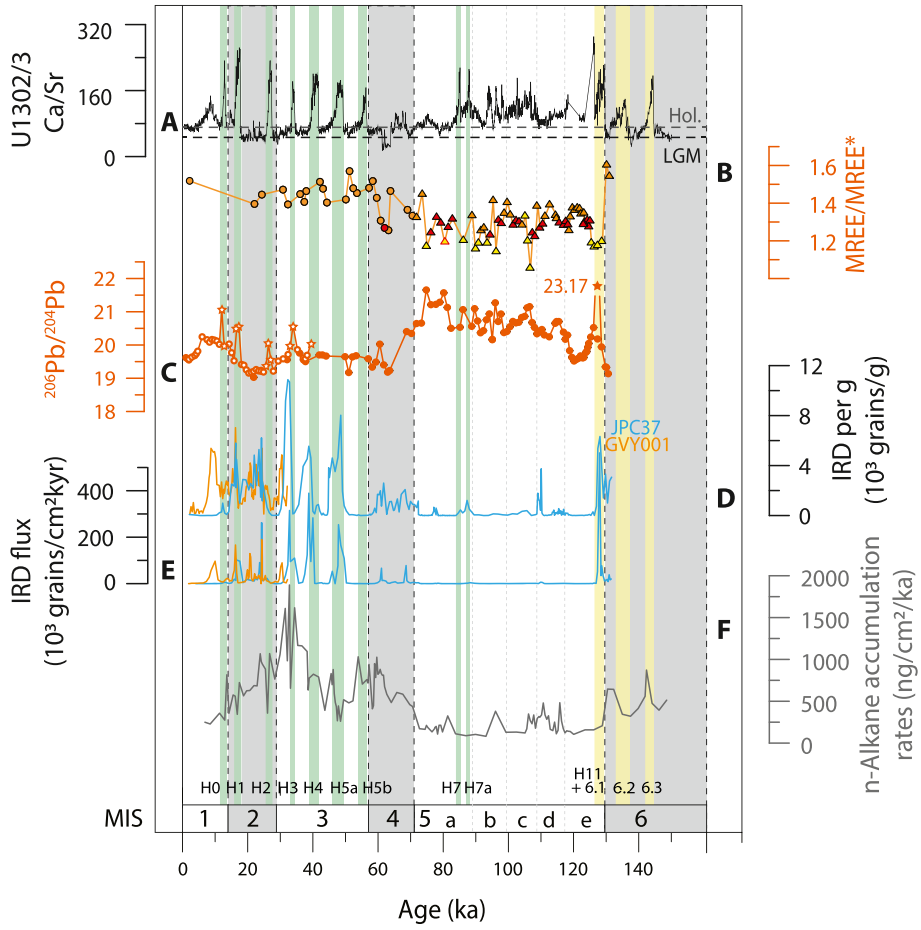

Fig. 8. Palaeoclimate records spanning marine isotope stages (MIS) 6–1: **(A)** Orphan Knoll IODP Site U1302/3 XRF scanning Ca/Sr ratios (Channell et al., 2012) with late Holocene and LGM values highlighted by horizontal dashed lines; **(B)** MREE/MREE* elemental ratios of authigenic Fe–Mn oxyhydroxides fractions of Site U1302/3 sediments. Data symbols correspond to those plotted in Fig. 8; **(C)** Site U1302/3 authigenic Fe–Mn oxyhydroxides $^{206}Pb/^{204}Pb$ isotope ratios; **(D)** IRD concentrations (Zhou et al., 2021) and **(E)** IRD flux (Zhou et al., 2021) for Orphan Knoll sediment cores JPC37 (blue) and GVY001 (orange); **(F)** North American-sourced aeolian dust deposition at IODP Site U1313 (~41°N) as tracked by n-alkane accumulation rates – the organic fraction of dust (Naafs et al., 2012). Trends in both $^{206}Pb/^{204}Pb$ and $^{208}Pb/^{204}Pb$ are consistent with the Pb isotopic composition of North American aeolian dust. Solid circles/stars = this study; open circles/stars = Crocket et al. (2012). MIS cold (warm) stages highlighted by vertical light grey (white) bars. Heinrich (detrital) layers preserved in both the Labrador Sea (identified using core-scanning-derived XRF Ca/Sr ratios by Channell et al. (2012) and subpolar North Atlantic sediments (Hemming, 2004; Hodell et al., 2008) are shown by labelled vertical light green bars. Labelled vertical light-yellow bars highlight Heinrich-like detrital layers where deposition was restricted to the Labrador Sea (Channell et al., 2012; Hodell et al., 2008). Star-shaped symbols denote Pb isotope data from U1302/3 Heinrich layers. See Fig. 1 for site locations. (For interpretation of the references to colour in this figure legend, the reader is referred to the Web version of this article.)

which it suppressed the delivery of weathered Pb from the interior of North America to Site U1302/3, at least immediately prior to the end of the PGM, were comparable to that of its LGM counterpart.

The radiogenic peak in the U1302/3 record during the last deglaciation is argued either to reflect incongruent weathering of highly reactive weakly-chemically altered glacial debris exposed following ice-sheet retreat (Crocket et al., 2012) or enhanced sourcing of weakly-weathered SP radiogenic material exposed following LIS retreat (Blaser et al., 2020). The overprint of H-layer deposition during T2 (the 'so-called' H11) in our Pb isotope data partially masks the equivalent weathering and runoff signal for the MIS 6/5e transition (Pb isotope zone β in Fig. 5c–e; Fig. 10). There is, however, no evidence in our records that the radiogenic supply of Pb from the interior of North America continued beyond ~122 ka. This is because the Pb isotope values in all our authigenic records return to compositions observed during the late Holocene by this time (as recorded at the transition between Pb isotope zones β and γ in Fig. 5c). The restriction of H-layer deposition to the Labrador Sea during MIS 6 (Naafs et al., 2013; Obrochta et al., 2014) points towards large differences in ice-mass distribution and ice-stream dynamics between the PGM and LGM LIS in the Hudson Bay area. The absence of detrital limestone-bearing H-layers in the central subpolar North Atlantic during MIS 6 has been attributed to a relatively thin (and therefore less voluminous) LIS that was cold-based and unable to generate H-events through surging of its Hudson Bay ice-stream (Obrochta et al., 2014). In this scenario, physical erosion of the SP terrane would have been reduced during the PGM relative to the LGM, leaving behind comparatively less-weakly weathered radiogenic material available to be chemically weathered following LIS retreat during T2. This may therefore explain the shorter time over which radiogenic values are a feature of our record during the MIS 6/5 transition (over no more than ~7 kyr) compared to the last deglaciation (~17 kyr) (compare width of horizontal black bars in Fig. 5c; Fig. 10).

The relatively short time over which radiogenic values are a feature of authigenic Pb isotope records during T2 and T1 support the idea that incongruent weathering did not play a leading role in changes in the Pb isotope composition of seawater bathing Orphan Knoll during LIS retreat. This is because it has been shown that any incongruent weathering signal should take tens of thousands of years to decay (Harlavan et al., 1998; Süfke et al., 2019), not ~3–5 kyr as we observe at U1302/3 (Fig. 5c–e). Furthermore, leaching

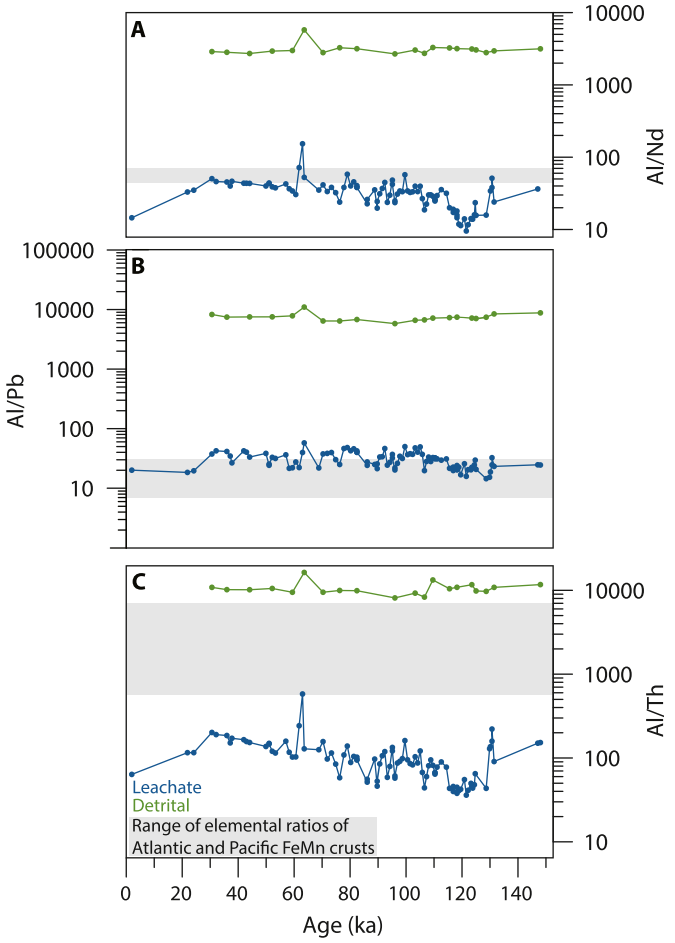

Fig. 9. Elemental ratios of: **(A)** Al/Nd, **(B)** Al/Pb and **(C)** Al/Th of leachate (blue) and detrital sediment (green) fractions from IODP Site U1302/3. Note the log scale of y-axis. Grey boxes define the range of elemental ratios associated with Atlantic and Pacific Fe–Mn crusts (Hein et al., 1999). (For interpretation of the references to colour in this figure legend, the reader is referred to the Web version of this article.)

experiments on granitic rock from the Swiss Alps show that increases in the $^{208}Pb/^{204}Pb$ ratios of the solute products of incongruent weathering should also lag those in $^{207}Pb/^{204}Pb$ because the main source of radiogenic ^{208}Pb (Th-bearing minerals) is more resistant to dissolution than (U-bearing) mineral sources of ^{206}Pb and ^{207}Pb (Dausmann et al., 2019; Süfke et al., 2019). Yet, all three authigenic Pb isotope ratios from U1302/3 increase at the same time during both T2 and T1 (Fig. 5c–e).

Independent reconstructions of LIS extent since the LGM highlight that while it began to retreat from ~20 ka (and seemingly first in Long Island Sound, Connecticut), a significant proportion of the SP was likely to have remained glaciated during T1 until ~12 ka (e.g., Dalton et al., 2020). If enhanced chemical weathering of SP craton was responsible for the radiogenic trends in U1302/3 authigenic Pb isotope data during T2 and T1, we might therefore expect these data to record only the more advanced stages of LIS retreat. Yet during T1, authigenic Pb isotope values at U1302/3 first began to increase ~20 ka (Fig. 5c–e). This disparity may highlight an important role for incongruent weathering in driving changes in the Pb isotope composition of bottom-waters bathing Orphan Knoll during the early stages of LIS retreat. Alternatively, the onset of radiogenic values at U1302/3 from ~20 ka and at ~130 ka during T2 may reflect an increase in microorganism-mediated chemical weathering of the SP beneath the LIS (cf. Wadham et al., 2010) and its runoff as it shifted from a cold-based to warm-based ice sheet (cf. Gutjahr et al., 2014). We infer that if there is an incongruent weathering influence on the Pb isotope composition of seawater bathing Orphan Knoll during LIS deglaciation its role may have been subordinate to that of changes in Pb provenance.

The T2 radiogenic spikes in our authigenic Pb isotope records correlate with the deposition at our study site of a red detrital layer sourced from Hudson Bay during a glacial outburst flood (Nicholl et al., 2012). This layer is argued to be the product of extensive deglaciation of the Hudson Bay region (Nicholl et al., 2012). We further note that the peak of radiogenic Pb supply to U1302/3 during the early Holocene is also broadly coincident with the final outburst of glacial Lake Agassiz-Ojibway south of Hudson Bay that most recent estimates suggest to have occurred between 8.7 (Dalton et al., 2020; Süfke et al., 2022) and 8.15 ka (Brouard et al., 2021). While these radiogenic spikes in Pb runoff to our study site cannot provide us with a precise understanding of the regional history of LIS retreat during T1 and T2, their respective durations may actually therefore provide us with a stratigraphic marker for the timing of collapse of the Hudson Bay Ice Saddle (or at least a likely latest possible date for it). This is argued to have occurred faster following the PGM than it did following the LGM, and in response to greater boreal summer insolation forcing (Carlson et al., 2008).

4.3.2. MIS 5 LIS history

The sudden return to elevated radiogenic Pb isotope values between ~115 and 75 ka during MIS 5d-a following the start of the LGC is arguably the most notable feature of our new dataset (Pb isotope zone δ in Fig. 5c–e). If a change in Pb provenance is involved, it cannot be attributed to, e.g., an increase in chemical weathering of exposed Greenland bedrock (e.g., the Ketilidian Mobile Belt) due to a diminished Greenland Ice Sheet. This is because the only circum-North Atlantic bedrock sufficiently radiogenic to explain these values is the greenstone belts of the SP (Fig. 2). Numerical ice-sheet modelling also shows that Greenland Ice Sheet regrowth following MIS 5e would have been relatively rapid (Kleman et al., 2013; Colleoni et al., 2014). Furthermore, it is challenging to explain the origin of this highly radiogenic interval by invoking continued chemical weathering (incongruent or otherwise) of weakly-chemically altered glacial debris on North America exposed following PGM LIS retreat because Pb isotope values recover to late Holocene-like values during the latter half of MIS 5e (by ~122 ka; compare Pb isotope zones γ & ι in Fig. 5c–e). This observation shows that the radiogenic weathering signal sourced from North America during T2 had already been exhausted. Instead, we consider that two mechanisms acting in concert are likely responsible for the observed radiogenic increase: (1) MIS 5 Labrador Current invigoration and, (2) incipient LIS glaciation.

The Labrador Current contributes to the transport of dissolved Pb to U1302/3 and its flow was likely reinvigorated following MIS 5e (Mao et al., 2018). The elevated radiogenic Pb isotope signal that we observe between ~115 and ~75 ka may therefore reflect a long-term increase in Labrador Current flow speed. An increase in Labrador Current vigor would supply more Pb from inner parts of the Labrador Sea that under less vigorous flow rates would not make it to U1302/3 given the particle-reactive nature and short seawater residence time of Pb. While our knowledge of Pb isotope compositions of the SP remain somewhat limited, the highly radiogenic signal preserved by our records for the MIS 5d-a may itself provide indirect evidence that SP rocks are on average highly radiogenic. Numerical modelling by Batchelor et al. (2019) propose that the high grounds of the SP terrane (the Quebec/Labrador region) were glaciated during MIS 5. The highly radiogenic values in our records may therefore also reflect renewed glacial erosion of the SP in high

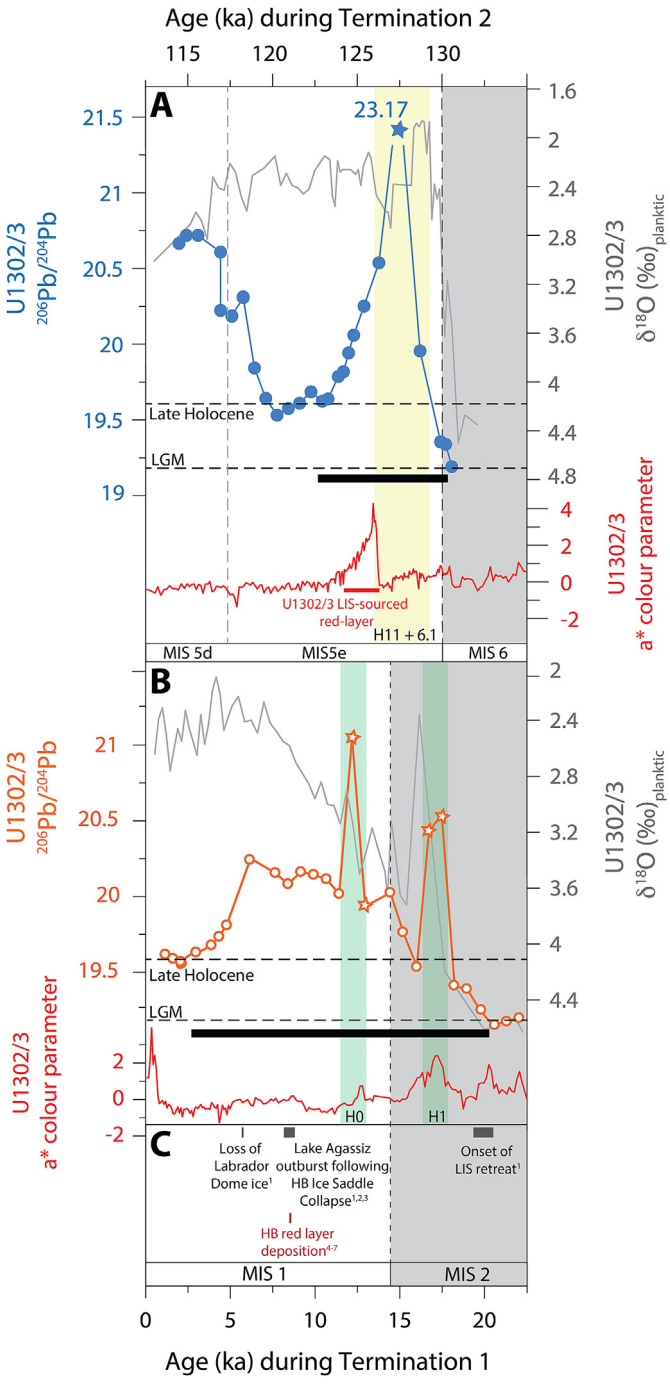

Fig. 10. The evolution of the Pb isotope composition of authigenic Fe–Mn oxyhydroxides from IODP Site U1302/3 during (**A**) Termination 2 and (**B**) Termination 1. (**C**) Laurentide Ice Sheet dynamics during Termination 1. Horizontal black bars highlight the duration of enhanced supply of dissolved radiogenic weathered material from the Superior Province craton exposed following Laurentide Ice Sheet following the onset of each termination. Dark grey horizontal bars highlight major evolution of the Laurentide Ice Sheet, where 1 = Dalton et al. (2020), 2 = Brouard et al. (2021), 3 = Margold et al. (2018), 8 = Dyke et al., 2002. Red layer depicted by red horizontal bar; 4 = Barber et al. (1999), 5 = Lajeunesse and St-Onge (2008), 6 = Jennings et al. (2015), 7 = Lochte et al. (2019). Solid circles/stars = this study; open circle/stars = Crocket et al. (2012). MIS cold (warm) stages are shown by vertical light grey (white) bars. Heinrich (detrital) layers preserved in both the Labrador Sea (identified using U1302/3 core-scanning-derived XRF Ca/Sr ratios by Channell et al. (2012) and subpolar North Atlantic sediments (Hemming, 2004; Hodell et al., 2008) are shown by labelled vertical light green bars. Labelled vertical light-yellow bars highlight Heinrich-like detrital layers where deposition was restricted to the Labrador Sea (Channell et al., 2012; Hodell et al., 2008). Horizontal dashed lines in (A) and (B) highlight Pb isotopes

regions where glaciation was not extensive enough to prevent chemical weathering of their glacial outwash products and the dissolved transport of its signal to the Labrador Sea. The delivery of such highly radiogenic material to the Labrador Sea would have been facilitated by Labrador Current invigoration, but also by the fact that these early glacial ice-caps were wet-based (so were not frozen to the substrate), which may have resulted in the highest delivery rates of dissolved SP materials to our study site the past ~130 kyr. If this argument is correct, it implies that both retreating and expanding continental ice-sheets are capable of facilitating elevated physicochemical weathering rates and associated runoff provided they coincide with relatively high precipitation rates as we might still expect during the relatively warm climate of MIS 5. We further note that this argument would hold up if the resultant elevated freshwater runoff at this time did not weaken the Labrador Current to the extent that it reduced the overall supply of radiogenic Pb to Orphan Knoll.

4.3.3. MIS 4 LIS history

The pronounced decline in Pb isotope values across the MIS 5a/4 transition from ~20.6 to ~19.3 $^{206}Pb/^{204}Pb$ (Pb isotope zone ε in Fig. 5c) most likely reflects a decrease in Labrador Current vigour (Mao et al., 2018). This decline also likely reflects an increase in deposition of North American-sourced aeolian dust (Fig. 8f), which has a relatively unradiogenic source signature (Lang et al., 2014; Jardine et al., 2021, Fig. 2) and a significant reduction in the supply of weathered Pb from the SP craton as the spatial footprint of the LIS increased notably for the first time during the LGC. This decline in Pb isotope ratios is also associated with the first sea-level lowstand of the LGC (compare panels a and c-e in Fig. 5) so likely documents a significant advance of the LIS across the SP and Hudson Bay. The 75 cm (~5.2 kyr) gap in our record spanning 10.05–10.80 mcd prevents us from establishing the exact timing of LIS advance in Hudson Bay during MIS 4. Regardless, the unradiogenic trend in our Pb isotope records at this time most likely reflects the westward advance of the Quebec-Labrador dome over Hudson Bay inferred for this time from till fabrics and lineation swarms in the Hudson Bay Lowlands (Kleman et al., 2010; Gauthier et al., 2019). Using GIA modelling, Pico et al. (2017) conclude that relative high MIS 3 sea-level along the US mid-Atlantic is most consistent with a scenario where the eastern Labrador (Quebec) sector of the LIS is ice-free between ~80 and 44 ka (MIS 5a to MIS 3). Our data strongly imply, however, that the eastern LIS expanded significantly over the SP craton across the MIS 5/4 transition and that their choice of ice-sheet configuration for MIS 4 in northeast North America is likely to be incorrect.

4.3.4. MIS 3 LIS history and implications for H-event mechanisms

The subsequent increase in U1302/3 Pb isotope ratios across the MIS 4/3 transition (e.g., of ~0.3 in $^{206}Pb/^{204}Pb$; Pb isotope zone ε in Fig. 5c) shows that the onset of MIS 3 is associated with increased delivery of radiogenic Pb to the Labrador Sea relative to MIS 4, perhaps enhanced by a strengthened Labrador Current (Mao et al., 2018). Excluding H-events, the values in our $^{206}Pb/^{204}Pb$ and $^{208}Pb/^{204}Pb$ records are persistently late Holocene-like (e.g., ~19.5 in $^{206}Pb/^{204}Pb$ and ~40 in $^{208}Pb/^{204}Pb$) throughout MIS 3 (see Figs. 2 and 5) before decreasing towards an LGM unradiogenic minima (e.g., of ~19.2 $^{206}Pb/^{204}Pb$ and ~39.5 $^{208}Pb/^{204}Pb$) over ~5 kyr from ~25 ka. These relatively radiogenic MIS 3 values were also recorded in the Crocket et al. (2012) Pb isotope records for Site U1302/3 between 25 and 37 ka, and have previously been interpreted by

values. (For interpretation of the references to colour in this figure legend, the reader is referred to the Web version of this article.)

Blaser et al. (2020) to mean that Hudson Bay was ice-free during this time.

Widespread deglaciation of Hudson Bay, the Hudson Bay Lowlands and the eastern Quebec-Labrador-sector of the LIS has also been hypothesized for MIS 3 by Dalton et al. (2019) based on a new stratigraphic fraemwork for the Hudson Bay Lowlands and their synthesis and re-interpretation of late Pleistocene geochronological data largely assembled by Dyke (2002). If the spatial extent of the LIS was significantly reduced at this time, we might expect to see clear evidence of a large spike in radiogenic Pb runoff during the MIS 4/3 transition (i.e., as is recorded for T2 and T1 at U1302/3, Fig. 10) in response to an increase in chemical weathering rates inland on North America. A short-lived radiogenic spike is potentially evident in our Pb isotope records at ~61 ka (see black stars in Fig. 5c–e), but it is much smaller than those associated with our study site for the last two deglaciations. This observation may indicate LIS retreat across MIS 4/3 reflects a failed termination of sorts (see also Schaefer et al., 2015) but the hydrological cycle remained largely sluggish resulting in a diminished chemical weathering response in North America, whether incongruent or otherwise. Yet, the corresponding $^{207}Pb/^{204}Pb$ isotope ratios of deep water bathing our study site during MIS 3, which are more unradiogenic than their late Holocene counterparts (by ~0.1, Fig. 5d), may highlight that a different explanation is required.

If the LIS did not retreat markedly during the MIS 4/3 transition (as argued by, e.g., Miller and Andrews, 2019), the only non-North American-based regional source that could potentially explain the Pb isotope composition of the deep-waters bathing our study site during MIS 3 is the Ketilidian Mobile Belt of southern Greenland (Fig. 2). West Greenland Ice Sheet retreat during MIS 3 has recently been inferred from a multi-proxy study of southern Davis Strait sediments (Siedenkrantz et al., 2019). Our data may therefore suggest that Greenland Ice Sheet retreat during this time could have also included the deglaciation and intensification in chemical weathering of the southern tip of this landmass.

5. Conclusions

We present new high-resolution records of authigenic Fe–Mn oxyhydroxide-derived Pb isotopes from Orphan Knoll IODP Site U1302/3 for the past ~130 kyr. We combine these new records with previously published Pb isotope data from this site spanning MIS 3–1 (Crocket et al., 2012) to track temporal variability in the input of Pb sourced from chemical weathering of the adjacent landmasses and its runoff to the Labrador Sea over the past ~130 kyr, which we argue predominantly varied as a function of Laurentide Ice Sheet extent in Hudson Bay.

We propose that the relatively short duration over which Fe–Mn authigenic Pb isotope compositions of bottom waters at U1302/3 during the MIS 6/5e transition are characterised by highly radiogenic values most likely reflects that Laurentide Ice Sheet retreat northwards across the Superior Province during Termination 2 was relatively rapid compared to Termination 1, and in response to greater boreal summer insolation forcing. The renewed existence and runoff of radiogenic Pb to the Labrador Sea during MIS 5d-a is recorded by the highest Pb isotope values in our data, which we argue most likely reflects invigoration of the Labrador Current and incipient glaciation and renewed glacial erosion of high grounds of the eastern Superior Province craton by wet-based localised ice-caps, most probably in the Quebec/Labrador region.

A subsequent large decrease in Pb isotope values towards unradiogenic LGM-like compositions between ~75 and 65 ka across the MIS 5/4 transition reflects an increase in North American glacial aeolian dust deposition, Labrador Current slow-down and a reduction in chemical weathering and runoff of Pb from North America due to westward advance of the Laurentide Ice Sheet across Hudson Bay. The relatively radiogenic Pb isotope composition of bottom-waters bathing our study site reported by Crocket et al. (2012) for MIS 3 has previously been argued to reflect that Laurentide Ice Sheet extent in Hudson Bay was significantly reduced at this time compared to the Last Glacial Maximum (Blaser et al., 2019). The relatively unradiogenic composition of authigenic $^{207}Pb/^{204}Pb$ ratios for our study site during MIS 3 (~0.1 lower) relative to the late Holocene highlights, however, that this interpretation may be incorrect. Instead, we propose that Laurentide Ice Sheet extent in Hudson Bay, and the Pb composition of runoff from this region of North America into the Labrador Sea, may not have changed significantly during MIS 3 compared to MIS 4 (cf. Miller and Andrews, 2019). Under this scenario, only southern Greenland Ice Sheet retreat, as recently inferred for this interval (Siedenkrantz et al., 2019), could explain the Pb isotope signature of seawater bathing U1302/3 during this time through increased chemical weathering of the Ketilidian Mobile Belt and Pb runoff from Greenland.

Data availability

The new IODP Site U1302/3 data presented and compiled Superior Province Pb isotope data are available in the attached Excel spreadsheets. Supplement 1 and 2 is also deposited in PANGAEA.

Author contributions

All authors contributed to the discussion of ideas presented in the manuscript. RLP acquired funding, generated the U1302/3 data and wrote the manuscript; IB designed the study, supervised RLP and co-wrote the manuscript; GLF, PAW and MG contributed to manuscript writing; MJC, AM, JAM helped to generate Pb isotopes and rare earth element data, oversaw instrumentation and helped with analysis. PAW co-supervised RLP.

Declaration of competing interest

The authors declare that they have no known competing financial interests or personal relationships that could have appeared to influence the work reported in this paper.

Acknowledgements

This research uses samples provided by the IODP, which is sponsored by the U.S. National Science Foundation and participating countries under management of Joint Oceanographic Institutions, Inc. We thank the shipboard party of IODP Expedition 303 and A. Wuelbers, W. Hale and H. Kuhlmann for their help at the Bremen Core Repository and Megan Spencer for laboratory support in Southampton. R.L.P. acknowledges funding from a University of Exeter International Excellence Scholarship. P.A.W. acknowledges support from Natural Environment Research Council (grant number NE/K014137/1) and the Royal Society (Wolfson Merit Award). We thank Antje Voelker for editorial handling and Nathalie Fagel and Alberto Reyes for constructive feedback at the review stage that helped significantly to improve the final version of this manuscript. We are also grateful to Nathalie Fagel for providing us with access to her compilations of circum-North Atlantic terrane Pb isotope data.

Appendix A. Supplementary data

Supplementary data to this article can be found online at https://doi.org/10.1016/j.quascirev.2022.107564.

References

Abbott, A.N., Haley, B.A., McManus, J., Reimers, C.E., 2015. The sedimentary flux of dissolved rare earth elements to the ocean. Geochim. Cosmochim. Acta 154, 186–200. https://doi.org/10.1016/j.gca.2015.01.010.

Abe-Ouchi, A., Saito, F., Kawamura, K., Raymo, M.E., Okuno, J.I., Takahashi, K., Blatter, H., 2013. Insolation-driven 100,000-year glacial cycles and hysteresis of ice-sheet volume. Nature 500, 190–193.

Aksu, A.E., Hiscott, R.N., 1992. Shingled Quaternary debris flow lenses on the northeast Newfoundland Slope. Sedimentology 39 (2), 193–206.

Aleinikoff, J.N., Muhs, D.R., Bettis III, E.A., Johnson, W.C., Fanning, C.M., Benton, R., 2009. Isotopic evidence for the diversity of late Quaternary loess in Nebraska: glaciogenic and nonglaciogenic sources. Geol. Soc. Am. Bull. 120 (11/12), 1362–1377. https://doi.org/10.1130/B26222.1.

Andreasen, R., Peate, D.W., Brooks, C.K., 2004. Magma plumbing systems in large igneous provinces; inferences from cyclical variations in Paleocene east Greenland basalts. Contrib. Mineral. Petrol. 147, 438–452.

Antonioli, F., Furlani, S., Montagna, P., Stocchi, P., 2021. The use of submerged speleothems for sea level studies in the mediterranean sea: a new perspective using glacial isostatic adjustment (GIA). Geosciences 11 (2), 77. https://doi.org/10.3390/geosciences11020077.

Arcuri, G.A., Dickin, A.P., 2018. Pb isotope mapping of paleoproterozoic gneisses in the SW grenville Province: evidence for a cryptic continental suture. Geosciences 8, 247. https://doi.org/10.3390/geosciences8070247.

Ashwal, L.D., Wooden, J.L., Emslie, R.F., 1986. Sr, Nd and Pb isotopes in Proterozoic instrusives astride the Grenville Front in Labrador: implications for crustal contamination and basement mapping. Geochim. Cosmochim. Acta 50, 2571–2585.

Baadsgaard, H., Collerson, K.D., Bridgwater, D., 1979. The Archaean gneiss complex of northern Labrador. 1. Preliminary U–Th–Pb geochronology. Can. J. Earth Sci. 16 (4), 951–961.

Baadsgaard, H., Nutman, A.P., Rosing, M., Bridgwater, D., Longstaffe, F.J., 1986. Alteration and metamorphism of Amitsoq gneisses from the Isukasia area, West Greenland: Recommendations for isotope studies of the early crust. Geochim. Cosmochim. Acta 50, 2165–2172.

Bailey, I., Hole, G.M., Foster, G.L., Wilson, P.A., Storey, C.D., Trueman, C.N., Raymo, M.E., 2013. An alternative suggestion for the Pliocene onset of major northern hemisphere glaciation based the geochemical provenance of North Atlantic Ocean ice-rafted debris. Quat. Sci. Rev. 75, 181–194. https://doi.org/10.1016/j.quascirev.2013.06.004.

Baker, J., M Peate, D., Waight, T., Meyzen, C., 2004. Pb isotopic analysis of standards and samples using a ^{207}Pb–^{204}Pb double spike and thallium to correct for mass bias with a double-focusing MC-ICP-MS. Chem. Geol. 211 (3–4), 275–303.

Barber, D.C., Dyke, A., Hillaire-Marcel, C., Jennings, A.E., Andrews, J.T., Kerwin, M.W., Bilodeau, G., McNeely, R., Southon, J., Morehead, M.D., Gagnon, J.M., 1999. Forcing of the cold event of 8,200 years ago by catastrophic drainage of Laurentide lakes. Nature 400, 344–348. https://doi.org/10.1038/22504.

Bard, E., Antonioli, F., Silenzi, S., 2002. Sea-level during the penultimate interglacial period based on a submerged stalagmite from Argentarola Cave (Italy). EPSL 196, 135–146.

Barker, A.K., Baker, J.A., Peate, D.W., 2006. Interaction of the rifting East Greenland margin with a zoned ancestral Iceland plume. Geology 34 (6), 481–484. https://doi.org/10.1130/G22366.1.

Batchelor, C.L., Margold, M., Krapp, M., Murton, D., Dalton, A.S., Gibbard, P.L., Stokes, C.R., Murton, J.B., Manica, A., 2019. The configuration of Northern Hemisphere ice sheets through the Quaternary. Nat. Commun. 10 (10). https://doi.org/10.1038/s41467-019-11601-2.

Bau, M., Schmidt, K., Koschinsky, A., Hein, J., Kuhn, T., Usui, A., 2014. Discriminating between different genetic types of marine ferro-manganese crusts and nodules based on rare earth elements and yttrium. Chem. Geol. 381, 1–9. https://doi.org/10.1016/j.chemgeo.2014.05.004.

Blake-Mizen, K.R., Hatfield, R.G., Stoner, J.S., Carlson, A.E., Xuan, C., Walczak, M.H., Lawrence, K.T., Channell, J.E.T., Bailey, I., 2019. Southern Greenland glaciation and western boundary undercurrent evolution recorded on Eirik Drift during the late Pliocene intensification of Northern Hemisphere glaciation. Quat. Sci. Rev. 209, 40–51.

Blaser, P., Lippold, J., Gutjahr, M., Frank, N., Link, J.M., Frank, M., 2016. Extracting foraminiferal seawater Nd isotope signatures from bulk deep sea sediment by chemical leaching. Chem. Geol. (439), 189–204.

Blaser, P., Pöppelmeier, F., Schulz, H., Gutjahr, M., Frank, M., Lippold, J., Heinrich, H., Link, J.M., Hoffmann, J., Szidat, S., Frank, N., 2019. The resilience and sensitivity of Northeast Atlantic deep water εNd to overprinting by detrital fluxes over the past 30,000 years. Geochem. Cosmochim. Acta (245), 79–97.

Blaser, P., Gutjahr, M., Pöppelmeier, F., Frank, M., Kaboth-Bahr, S., Lippold, J., 2020. Labrador Sea bottom water provenance and REE exchange during the past 35,000 years. EPSL 542, 116299.

Brouard, E., Roy, M., Godbout, P.-M., Veillette, J.J., 2021. A framework for the timing of the final meltwater outburts from glacial Lake Agassiz-Ojibway. Quat. Scr. Rev. 274, 107269.

Channell, J.E.T., Kanarnatsu, T., Sato, T., Stein, R., Alvarez Zarikian, C.A., Malone, M.J., 2006. Sites U1302 and U1303. In: Proceedings of the IODP, 303/306. Integrated Ocean Drilling Program Management), College Station TX.

Channell, J.E.T., Xuan, C., Hodell, D.A., 2009. Stacking paleointensity and oxygen isotope data for the last 1.5 Myrs (PISO-1500). Earth Planet Sci. Lett. 283, 14–23.

Carlson, A.E., LeGrande, A.N., Oppo, D.W., Came, R.E., Schmidt, G.A, Anslow, F.S., Licciardi, J.M., Obbink, E.A, 2008. Rapid early Holocene deglaciation of the Laurentide ice sheet. Nat. Geosci. 1, 620–624. https://doi.org/10.1038/ngeo285.

Channell, J.E.T., Hodell, D.A., Romero, O., Hillaire-Marcel, C., de Vernal, A., Stoner, J.S., et al., 2012. A 750-kyr detrital-layer stratigraphy for the north atlantic (IODP sites U1302-U1303, orphan Knoll, Labrador Sea). Earth Planet Sci. Lett. (317–318), 218–230.

Colleoni, F., Liakka, J., Krinner, G., Jakobsson, M., Masina, S., Peyaud, V., 2011. The sensitivity of the Late Saalian (140 ka) and LGM (21 ka) Eurasian ice sheets to sea surface conditions. Clim. Dynam. 37, 531–553.

Colleoni, F., Masina, S., Cherchi, A., Iovino, D., 2014. Impact of orbital parameters and greenhouse gas on the climate of MIS 7 and MIS 5 glacial inceptions. J. Clim. 27, 8918–8933.

Colleoni, F., Wekerle, C., Neaslund, J.-O., Brandefelt, J., Masina, S., 2016. Constraint on the penultimate glacial maximum Northern Hemisphere ice topography (~140 kyrs BP). Quat. Sci. Rev. 137, 97–112.

Crocket, K.C., Vance, D., Foster, G.L., Richards, D.A., Tranter, M., 2012. Continental weathering fluxes during the last glacial/interglacial cycle: insights from the marine sedimentary Pb isotope record at Orphan Knoll, NW Atlantic. Quat. Sci. Rev. 30, 89–99.

Crocket, K.C., Hill, E., Abell, R.E., Johnson, C., Gary, S.F., Brand, T., Hathorne, E.C., 2018. Rare Earth element distribution in the NE Atlantic: evidence for benthic sources, longevity of the seawater signal, and biogeochemical cycling. Front. Mar. Sci. 5. https://doi.org/10.3389/fmars.2018.00147.

Dalton, A.S., Finkelstein, S.A., Barnett, P.J., Forman, S.L., 2016. Constraining the late Pleistocene history of the Laurentide ice sheet by dating the Missinaibi Formation, Hudson Bay Lowlands, Canada. Quat. Sci. Rev. 146, 288–299.

Dalton, A.S., Margold, M., Stokes, C.R., et al., 2020. An updated radiocarbon-based ice margin chronology for the last deglaciation of the North American Ice Sheet Complex. Quat. Sci. Rev. 234, 106223. https://doi.org/10.1016/j.quascirev.2020.106223.

Dalton, A.S., S Finkelstein, S.A., Barnett, P.J., Valiranta, M., Forman, S.L., 2017. Late Pleistocene chronology, palaeoecology and stratigraphy at a suite of sites along the Albany River, Hudson Bay lowlands, Canada. Palaeogeogr. Palaeoclimatol. Palaeoecol. 492, 50–63.

Dalton, A.S., Finkelstein, S.A., Forman, S.L., Barnett, P.J., Pico, T., Mitrovica, J.X., 2019. Was the Laurentide ice sheet significantly reduced during Marine Isotope Stage 3? Geology 47, 111–114.

Dausmann, V., Gutjahr, M., Frank, M., Kouzmanov, K., Schaltegger, U., 2019. Experimental evidence for mineral-controlled release of radiogenic Nd, Hf and Pb isotopes from granitic rocks during progressive chemical weathering. Chem. Geol. 507, 64–84. https://doi.org/10.1016/j.chemgeo.2018.12.024.

de Boer, B., Lourens, L., van de Wal, R.S., 2014. Persistent 400,000-year variability of Antarctic ice volume and the carbon cycle is revealed throughout the Plio-Pleistocene. Nat. Commun. 5, 2999. https://doi.org/10.1038/ncomms3999.

Dendy, S., Austermann, J., Creveling, J.R., Mitrovica, J.X., 2017. Sensitivity of Last Interglacial sea-level high stands to ice sheet configuration during Marine Isotope Stage 6. Quat. Sci. Rev. 171, 234–244.

Déry, S.J., Mlynowski, T.J., Hernández-Henríquez, M.A., Straneo, F., 2011. Interannual variability and interdecadal trends in Hudson Bay streamflow. J. Mar. Syst. 88, 341–351. https://doi.org/10.1016/j.jmarsys.2010.12.002.

Deschamps, P., Durand, N., Bard, E., Hamelin, B., Camoin, G., Thomas, A.L., Henderson, G.M., Okuno, J., Yokoyama, Y., 2012. Ice-sheet collapse and sea-level rise at the Bølling warming 14,600 years ago. Nature 483 (7391), 559–564. https://doi.org/10.1038/nature10902.

Doe, B.R., Delevaux, M.H., 1980. Lead-isotope investigations in the Minnesota River Valley– Late-tectonic and post tectonic granites. Geol. Soc. Am. Spec. Pap. 182, 105–112.

Dorale, J.A., Onac, B.P., Fornós, J.J., Ginés, J., Ginés, A., Tuccimei, P., Peate, D.W., 2010. sea-level highstand 81,000 Years ago in mallorca. Science 327 (5967), 860–863.

Du, J., Haley, B.A., Mix, A.C., 2016. Neodymium isotopes in authigenic phases, bottom waters and detrital sediments in the Gulf of Alaska and their implications for paleo-circulation reconstruction. Geochim. Cosmochim. Acta 193, 14–35. https://doi.org/10.1016/j.gca.2016.08.005.

Dwyer, B., Austermann, J., D'Andrea, W.J., Crell, R.C., Sandstrom, M.R., Cashman, M., Rovere, A., Raymo, M.E., 2021. Sea-level trends across the Bahamas constrain peak last interglacial ice melt. Proc. Natl. Acad. Sci. Unit. States Am. 118 (33), e202689118. https://doi.org/10.1073/pnas.2026839118.

Dyke, A.S., Andrews, J.T., Clark, P.U., England, J.H., Miller, G.H., Shaw, J., Veillette, J.J., 2002. The Laurentide and Innuitian ice sheets during the last glacial maximum. Quat. Sci. Rev. 21, 9–31.

Ehlers, J., Gibbard, P.L., Hughes, P.D. (Eds.), 2011. Quaternary Glaciation Extent and Chronology: a Closer Look. Developments in Quaternary Science 15. Elsevier, Amsterdam.

Elderfield, H., Ferretti, P., Greaves, M., Crowhurst, S., McCave, I.N., Hodell, D., Piotrowski, A.M., 2012. Evolution of ocean temperature and ice volume through the Mid-Pleistocene Climate Transition. Science 337, 704–709.

Ellam, R.M., Stuart, F.M., 2000. The sub-lithospheric source of North Atlantic basalts: evidence for, and significance of, a common end-member. J. Petrol. 41 (7), 919–932. https://doi.org/10.1093/petrology/41.7.919.

Expedition 303 Scientists, 2006. Site U1308. In: Channell, J.E.T., et al. (Eds.), North Atlantic Climate, Proc. Integr. Ocean Drill. Program, vol. 303. https://doi.org/10.2204/iodp.proc.303306.108.2006.

Fagel, N., Hillaire-Marcel, M., Humblet, R., Brasseur, D., Weis, R., Stevenson, R, 2004. Nd and Pb isotope signatures of the clay-size fraction of Labrador Sea sediments

during the Holocene: Implications for the inception of the modern deep circulation pattern. Paleoceanogr. Paleoclimatol. 19 (3), PA3002. https://doi.org/10.1029/2003PA000993.
Fagel, N., Innocent, C., Gariepy, C., Hillaire-Marcel, C., 2002. Sources of Labrador Sea sediments since the last glacial maximum inferred from Nd-Pb isotopes. Geochem. Cosmochim. Acta 66 (14), 2569–2581.
Fagel, N., Innocent, C., Stevenson, R.K., Hillaire-Marcel, C., 1999. Deep circulation changes in the Labrador Sea since the Last Glacial Maximum: New constraints from Sm-Nd data on sediments. Paleoceanography 14 (6), 777–788. https://doi.org/10.1029/1999PA900041.
Fagel, N., Mattielli, N., 2011. Holocene evolution of deep circulation in the northern North Atlantic traced by Sm, Nd and Pb isotopes and bulk sediment mineralogy. Paleoceanogr. Paleoclimatol. 26 (4), PA4220. https://doi.org/10.1029/2011PA002168.
Farmer, G.L., Barber, D., Andrews, J.T., 2003. Provenance of late quaternary ice-proximal sediments in the north atlantic: Nd, Sr and Pb isotopic evidence. Earth Planet Sci. Lett. 209, 227–243.
Foland, S.G., 1982. Geochemistry, Geochronology and Origin of an Archean Greenstone-Granite Terrain Wabigoon Subprovince Northwestern Ontario, p. 7500. Graduate Student Theses. Dissertations, & Professional Papers.
Foster, G.L., Vance, D., 2006. Negligible glacial–interglacial variation in continental chemical weathering rates. Nature 444, 918–921.
Frank, M., 2002. Radiogenic isotopes: tracers of past ocean circulation and erosional input. Rev. Geophys. 40, 1001. https://doi.org/10.1029/2000RG000094.
Gale, A., Dalton, C.A., Langmuir, C.H., Su, Y., Schilling, J.-G., 2013. The mean composition of ocean ridge basalts. Geochem. Geophys. Geosyst. 14, 489–518. https://doi.org/10.1029/2012GC004334.
Gariepy, C., Allegre, C.J., 1985. The lead isotope geochemistry and geochronology of late-kinematic intrusives from the Abitibi greenstone belt, and the implications for late Archean crustal evolution. Geochim. Cosmochim. Acta 49, 237 1–2383.
Gauthier, M.S., Hoer, T.J., Ross, M., Kelley, S.E., Rochester, A., McCausland, P., 2019. The subglacial mosaic of the Laurentide Ice Sheet; a study of the interior region of southwestern Hudson Bay. Quat. Sci. Rev. 214, 1–27.
Gowan, E.J., Zhang, X., Khosravi, S., et al., 2021. A new global ice sheet reconstruction for the past 80 000 years. Nat. Commun. 12, 1199. https://doi.org/10.1038/s41467-021-21469-w.
Grant, K.M., Rohling, E.J., Bar-Matthews, M., Ayalon, A., Medina-Elizalde, M., Bronk Ramsey, C., Satow, C., Roberts, A.P., 2012. Rapid coupling between ice volume and polar temperature over the past 150 000 years. Nature 491, 744–747. https://doi.org/10.1038/nature11593.
Grant, K.M., Rohling, E.J., Ramsey, C.B., Cheng, H., Edwards, R.L., Florindo, F., Heslop, D., Marra, F., Roberts, A.P., Tamisiea, M.E., Williams, F., 2014. Sea-level variability over five glacial cycles. Nat. Commun. 5, 5076.
Gutjahr, M., Frank, M., Lippold, J., Halliday, A.N., 2014. Peak Last Glacial weathering intensity on the North American continent recorded by the authigenic Hf isotope composition of North Atlantic deep-sea sediments. Quat. Sci. Rev. 99, 97–111. https://doi.org/10.1016/j.quascirev.2014.06.022.
Gutjahr, M., Frank, M., Stirling, C.H., Klemm, V., van de Flierdt, T., Halliday, A.N., 2007. Reliable extraction of a deepwater trace metal isotope signal from Fe-Mn oxyhydroxide coatings of marine sediments. Chem. Geol. 242 (3–4), 351–370.
Gutjahr, M., Frank, M., Halliday, A.N., Keigwin, L.D., 2009. Retreat of the Laurentide ice sheet tracked by the isotopic composition of Pb in western North Atlantic seawater during termination 1. Earth Planet Sci. Lett. 286, 546–555.
Haley, B.A., Klinkhammer, G.P., McManus, J., 2004. Rare earth elements in pore waters of marine sediments. Geochim. Cosmochim. Acta 68, 1265–1279. https://doi.org/10.1016/j.gca.2003.09.012.
Hansen, B.T., Friderichsen, J.D., 1989. The influence of recent lead loss on the interpretation of disturbed U-Pb systems in zircons from igneous rocks in East Greenland. Lithos 209–223.
Hansen, H., Nielsen, T.F.D., 1999. Crustal contamination in Paleogene East Greenland flood basalts: plumbing system evolution during continental rifting. Chem. Geol. 157, 89–188.
Harlavan, Y., Erel, Y., Blum, J.D., 1998. Systematic changes in lead isotopic composition with soil age in glacial granitic terrains. Geochim. Cosmochim. Acta 62, 33–46.
Hathorne, E.C., Stichel, T., Brück, B., Frank, M., 2015. Rare Earth element distribution in the Atlantic sector of the Southern Ocean: the balance between particle scavenging and vertical supply. Mar. Chem. 177, 157–171. https://doi.org/10.1016/j.marchem.2015.03.011.
Hein, J.R., Koschinsky, A., Bau, M., Manheim, F.T., Kang, J.-K., Roberts, L., 1999. Cobalt-rich ferromanganese crusts in the Pacific. In: Cronan, D.S. (Ed.), Handbook of Marine Mineral Deposits. CRC Press, pp. 239–279.
Hemming, S.R., 2004. Heinrich events: massive late Pleistocene detritus layers of the North Atlantic and their global climate imprint. Rev. Geophys. 42 (1). https://doi.org/10.1029/2003RG000128.
Henderson, G.M., Maier-Reimer, E., 2002. Advection and removal of 210Pb and stable Pb isotopes in the oceans: a general circulation model study. Geochim. Cos- mochim. Acta 66, 257–272. https://doi.org/10.1016/S0016-7037(01)00779-7.
Hibbert, F.D., Rohling, E.J., Dutton, A., Williams, F.H., Chutcharavan, P.M., Zhao, C., Tamisiea, M.E., 2016. Corals as indicators of past sea-level change: a global repository of U-series dated benchmarks. Quat. Sci. Rev. 145, 1–56.
Hillaire-Marcel, C., de Vernal, A., McKay, J.L., 2011. Foraminifer isotope study of the Pleistocene Labrador Sea, northwest North Atlantic (IODP Sites 1302/03 and 1305), with emphasis on paleoceanographical differences between its "inner" and "outer" basins. Mar. Geol. 279 (1–4), 188–198.
Hodell, D.A., Channell, J.E.T., Curtis, J.H., Romero, O.E., Rohl, U., 2008. Onset of "Hudson Strait" Heinrich events in the eastern North Atlantic at the end of the middle Pleistocene transition (<640 ka)? Paleoceanography 23, PA4218. https://doi.org/10.1029/2008PA001591.
Holm, P.M., 1988. Nd, Sr and Pb isotope geochemistry of the lower lavas, E Greenland tertiary igneous Province. In: Morton, A.C., Parson, L.M. (Eds.), Early Tertiary Volcanism and the Opening of the NE Atlantic, vol. 39. Geological Society Special Publications, pp. 181–195.
Innocent, C., Fagel, N., Stevenson, K., Hillaire-Marcel, C., 1997. Sm-Nd signature of modern and late Quaternary sediments from the northwest North Atlantic: Implications for deep current changes since the Last Glacial Maximum. Earth. Planet. Sci. Lett. 146 (3–4), 607–625.
Jardine, G.E., Crocker, A.J., Bailey, I., Cooper, M.J., Milton, J.A., Wilson, P.A., 2021. The imprint of windblown dust from the north American southwest on the California channel islands and Pacific Ocean sediments. Quat. Sci. Rev. 261, 106934. https://doi.org/10.1016/j.quascirev.2021.106934.
Jennings, A., Andrews, J., Pearce, C., Wilson, L., Sædís Ólfasdótttir, S., 2015. Detrital carbonate peaks on the Labrador shelf, a 13-7 ka template for freshwater forcing from the Hudson Strait outlet of the Laurentide Ice Sheet into the subpolar gyre. Quat. Sci. Rev. 107, 62–80. https://doi.org/10.1016/j.quascirev.2014.10.022.
Jensen, S.M., 1994. Lead isotope signatures of mineralized rocks in the Caledonian fold belt of North-East Greenland. App. Grønlands, geol. Under 162, 169–176.
Jochum, K.P., Weis, U., Schwager, B., Stoll, B., Wilson, S.A., Haug, G.H., Andreae, M.O., Enzweiler, J., 2016. Reference values following ISO guidelines for frequently requested rock reference materials. Geostand. Geoanal. Res. 40 (3), 333–350.
Kalsbeek, F., Taylor, P.N., 1985. Isotopic and chemical variation in granites across a Proterozic continental margin – the Ketilidian mobile belt of south Greenland. Earth Planet Sci. Lett. 73, 65–80.
Kalsbeek, F., Taylor, P.N., Henriksen, N., 1984. Age of rocks, structures, and metamorphism in the Nagssugtoqidian mobile belt, West Greenland – field and Pb-isotopic evidence. Can. J. Earth Sci. 21, 1126–1131.
Kalsbeek, F., Pidgeon, R.T., Taylor, P.N., 1987. Nagssugtoqidian mobile belt of West Greenland: a cryptic 1850 Ma suture between two Archaean continents–chemical and isotopic evidence. Earth Planet Sci. Lett. 85, 365–385.
Kalsbeek, F., Taylor, P.N., Pidgeon, R.T., 1988. Unreworked Archaean basement and Proterozoic supracrustal rocks from northeastern Disko Bugt, West Greenland: implications for the nature of Proterozoic mobile belts in Greenland. Can. J. Earth Sci. 25, 773–782.
Kalsbeek, F., Austrheim, H., Bridgwater, D., Hansen, B.T., Pedersen, S., Taylor, P.N., 1993. Geochronology of archaean and proterozoic events in the ammassalik area, south-east Greenland, and comparisons with the lewis ian of scotland and the nagssugtoqidian of west Greenland. Precambrian Res. 62, 239–270.
Kerr, P.J., Tassier-Surine, S.A., Kilgore, S.M., Bettis III, E.A., Dorale, J.A., Cramer, D.B., et al., 2021. Timing, provenance, and implications of two MIS 3 advances of the Laurentide ice sheet into the upper Mississippi river basin, USA. QSR 261, 106926.
Kleman, J., Jansson, K., De Angelis, H., Stroeven, A.P., Hattestrand, C., Alm, G., Glasser, N., 2010. North American Ice Sheet build-up during the last glacial cycle, 115–21 kyr. Quat. Sci. Rev. 29, 2036–2051. https://doi.org/10.1016/j.quascirev.2010.04.021.
Kleman, J., Fastook, J., Ebert, K., Nilsson, J., Caballero, R., 2013. Pre-LGM Northern Hemisphere ice sheet topography. Clim. Past. 9, 2365–2378. https://doi.org/10.5194/cp-9-2365-2013.
Klemm, V., Reynold, B., Frank, M., Pettke, T., Halliday, A.N., 2007. Cenozoic changes in atmospheric lead recorded in Central Pacific ferromanganese crusts. Earth Planet Sci. Lett. 253 (1–2), 57–66. https://doi.org/10.1016/j.epsl.2006.10.018.
Kopp, R.E., Simons, F.J., Mitrovica, J.X., Maloof, A.C., Oppenheimer, M.A., 2013. A probabilistic assessment of sea level variations within the last interglacial stage. Geophys. J. Int. 193 (2), 711–716. https://doi.org/10.1093/gji/ggt029.
Kurzweil, F., Gutjahr, M., Vance, D., Keigwin, L., 2010. Authigenic Pb isotopes from the Laurentian Fan: changes in chemical weathering and patterns of North American freshwater runoff during the last deglaciation. Earth Planet Sci. Lett. 299, 458–465. https://doi.org/10.1016/j.epsl.2010.09.031.
Lajeunesse, P., St-Onge, G., 2008. The subglacial origin of the Lake Agassiz-Ojibway final outburst flood. Nat. Geosci. 1, 184–188. https://doi.org/10.1038/ngeo130.
Lambeck, K., Purcell, A., Funder, S., Kjaer, K., Larsen, E., Möller, P., 2006. Constraints on the Late Saalian to early Middle Weichselian ice sheet of Eurasia from field data and rebound modelling. Boreas 35, 539–575.
Lambeck, K., Purcell, A., Zhao, J., Svensson, N.O., 2010. The Scandinavian Ice Sheet: from MIS 4 to the end of the last glacial maximum. Boreas 39, 410–435.
Lambeck, K., Purcell, A., Zhao, S., 2017. The North American Late Wisconsin ice sheet and mantle viscosity from glacial rebound analyses. Quat. Sci. Rev. 158, 172–210.
Lambeck, K., Rouby, H., Purcell, A., Sun, Y., Sambridge, M., 2014. Sea level and global ice volumes from the Last Glacial Maximum to the Holocene. Proc. Natl. Acad. Sci. Unit. States Am 111 (43), 15296–15303. https://doi.org/10.1073/pnas.1411762111.
Lang, D.C., Bailey, I., Wilson, P.A., Beer, C., Bolton, C.T., Newsam, C., Spencer, M.R., Friedrich, O., Gutjahr, M., Foster, G.L., Cooper, C.J., Milton, A., 2014. The transition on North America from the warm humid Pliocene to the glaciated Quaternary traced by eolian dust deposition at a benchmark North Atlantic Ocean drill site. Quat. Sci. Rev. 93C, 125e141. https://doi.org/10.1016/j.quascirev.2014.04.005.
Lisiecki, L.E., Raymo, M.E., 2005. A Pliocene-Pleistocene stack of 57 globally

distributed benthic δ 18O records. Paleoceanography 20 (1), 1–17.
Lisiecki, L.E., Raymo, M.E., 2009. Diachronous benthic $\delta^{18}O$ responses during late Plestocene terminations. Paleoceanography 24, PA3210.
Lochte, A.A., Repschläger, J., Kienast, M., Garbe-Schönberg, D., Andersen, N., Hamann, C., Schneider, R., 2019. Labrador Sea freshening at 8.5 ka BP caused by Hudson Bay ice saddle collapse. Nat. Commun. 10 (586), 1–9. https://doi.org/10.1038/s41467-019-08408-6.
Mao, L., Piper, D.J.W., Saint-Ange, F., Andrews, J.T., 2018. Labrador Current fluctuation during the last glacial cycle. Mar. Geol. 395, 234–246.
Margold, M., Stokes, C.R., Clark, C.D., 2018. Reconciling records of ice streaming and ice margin retreat to produce a palaeogeographic reconstruction of the deglaciation of the Laurentide Ice Sheet. Quat. Sci. Rev. 189, 1–30.
Martin, E.E., Blair, S.W., Kamenov, G.D., Scher, H.D., Bourbon, E., Basak, C., Newkirk, D.N., 2010. Extraction of Nd isotopes from bulk deep sea sediments for paleoceanographic studies on Cenozoic time scales. Chem. Geol. (269), 414–443.
Mathieu, L., Crepon, A., Kontak, D.J., 2020. Tonalite-dominated magmatism in the Abitibi subprovince, Canada, and significance for Cu-Au magmatic-hydrothermal systems. Minerals 10, 242. https://doi.org/10.3390/min10030242.
Miller, G.H., Andrews, J.T., 2019. Hudson Bay was not deglaciated during MIS-3. Quat. Sci. Rev. 225, 105944.
Montsion, R.M., Thurston, P., Ayer, J., 2018. 1:2 000 000 Scale Geological Compilation of the Superior Craton - Version 1. Mineral Exploration Research Centre, Harquail School of Earth Sciences, Laurentian University Document Number MERC-ME-2018-017.
Moorbath, S., Taylor, P.N., Goodwin, R., 1981. Origin of granitic magma by crustal remobilisation: Rb-Sr and Pb/Pb geochronology and isotope geochemistry of the late Archaean Qôqut Granite Complex of southern West Greenland. Geochim. Cosmochim. Acta 45, 1051–1060.
Naafs, B.D.A., Hefter, J., Acton, G., Haug, G.H., Martínez-Garcia, A., Pancost, R., Stein, R., 2012. Strengthening of north American dust sources during the late pliocene (2.7 Ma). Earth Planet Sci. Lett. 317–318, 8–19. https://doi.org/10.1016/j.epsl.2011.11.026.
Naafs, B.D.A., Hefter, J., Stein, R., 2013. Millennial-scale ice rafting events and Hudson Strait heinrich(-like) events during the late pliocene and Pleistocene: a review. QSR 80, 1–28.
Natural Resources Canada, 2006. Atlas of Canada Watershed Framework. https://www.nrcan.gc.ca/maps-tools-publications/tools/geodetic-reference-systems/water/16888. (Accessed 10 June 2021). Accessed.
Nicholl, J.A.L., Hodell, D.A., Naafs, B.D.A, Hillaire-Marcel, C., Channell, J.E.T., Romero, O.E., 2012. A Laurentide outburst flooding event dur-ing the last interglacial period. Nat. Geosci. 5, 901–904. https://doi.org/10.1038/ngeo1622.
Obrochta, S.P., Crowley, T.J., Channell, J.E.T., Hodell, D.A., Baker, P.A., Seki, A., Yokoyama, Y., 2014. Climate variability and ice-sheet dynamics during the last three glaciations. Earth Planet Sci. Lett. 406, 198–212.
Osborne, A.H., Hathorne, E.C., Schijf, J., Plancherel, Y., Böning, P., Frank, M., 2017. The potential of sedimentary foraminiferal rare earth element patterns to trace water masses in the past. Geochem. Geophys. Geosyst. 18, 1550–1568. https://doi.org/10.1002/2016GC006782.
Patton, G.M., Francois, R., Weis, D., Hathorne, E., Gutjahr, M., Frank, M., Gordon, K., 2021. An experimental investigation of the acquisition of Nd by authigenic phases of marine sediments. Geochmica et Cosmochimica Acta 301, 1–29. https://doi.org/10.1016/j.gca.2021.02.010.
Percival, J.A., 2007. Geology and metallogeny of the superior Province, Canada. In: Goodfellow, W.D. (Ed.), Mineral Deposits of Canada: A Synthesis of Major Deposit-Types, District Metallogeny, the Evolution of Geological Provinces, and Exploration Methods: Geological Association of Canada. Mineral Deposits Division, Special Publication.
Percival, J.A., Skulski, T., Sanborn-Barrie, M., Stott, G.M., Leclair, A.D., Corkery, M.T., Boily, M., 2012. Geology and tectonic evolution of the superior Province, Canada. Chapter 6. In: Percival, J.A., Cook, F.A., Clowes, R.M. (Eds.), Tectonic Styles in Canada: the LITHOPROBE Perspective. Geological Association of Canada, pp. 321–378. Special Paper 49.
Peterson, T.D., Esperanca, S., LeCheminant, A.N., 1994. Geochemistry and origin of the proterozoic ultrapotassic rocks of the churchill Province, Canada. Mineral. Petrol. 51, 251–276.
Pico, T., Creveling, J.R., Mitrovica, J.X., 2017. sea-level records from the U.S. Mid-atlantic constrain Laurentide ice sheet extent during marine isotope stage 3. Nat. Commun. 8, 15612. https://doi.org/10.1038/ncomms15612.
Piper, D.Z., 1974. Rare earth elements in the sedimentary cycle: a summary. Chem. Geol. 14, 285–304.
Potter, E.K., Lambeck, K., 2003. Reconciliation of sea-level observations in the Western North Atlantic during the last glacial cycle. Earth Planet Sci. Lett. 217, 171–181.
Rabineau, M., Berné, S., Olivet, J.L., Aslanian, D., Guillocheau, F., Joseph, P., 2006. Paleo sea levels reconsidered from direct observation of paleoshoreline position during Glacial Maxima (for the last 500,000 yr). Earth Planet Sci. Lett. 252, 119–137.
Reed, J.C., Wheeler, J.O., Tucholke, B.E., Card, K.D., Davidson, A., Hoffman, P.F., Okulitch, A.V., Palmer, A.R., Sanford, B.V., Williams, G.K., Williams, H., Dixon, J., Embry, A.F., Holcombe, T.L., Laine, E.P., Mountain, G.S., Popenoe, P., Wiley, T., 2005. Geologic Map of North America. Geological Society of America. Continent-Scale Map 001, scale 1:5,000,000.
Richardson, A.J., Hollings, P., Franklin, J.M., 2005. Geochemistry and radiogenic isotope characteristics of the sills of the nipigon embayment: lake nipigon region geoscience initiative. Ontario Geological Survey, Open File Report 6175, 88p.
Rohling, E.J., Foster, G.L., Grant, K.M., Marino, G., Roberts, A.P., Tamisiea, M.E., Williams, F., 2014. Sea-level and deep-sea-temperature variability over the past 5.3 million years. Nature 508, 477–482.
Rohling, E.J., Hibbert, F.D., Williams, F.H., Grant, K.M., Marino, G., Foster, G.L., Hennekam, R., de Lange, G.J., Roberts, A.P., Yu, J., Webster, J.M., Yokoyama, Y., 2017. Differences between the last two glacial maxima and implications for ice-sheet, $\delta^{18}O$, and sea-level reconstructions. Quat. Sci. Rev. 178, 1–28.
Saunders, A.D., Kempton, P.D., Fitton, J.G., Larsen, L.M., 1999. Sr, Nd, and Pb isotopes and trace element geochemistry of basalts from the Southeast Greenland margin. Proc. Ocean Drill. Progr. Sci. Results 163, 77–93.
Schaefer, J.M., et al., 2015. The southern glacial maximum 65,000 years ago and its unfinished termination. Quat. Sci. Rev. 114, 52–60.
Scharer, U., 1991. Rapid continental crust formation at 1.7 Ga from a reservoir with chondritic isotope signatures, eastern Labrador. Earth Planet Sci. Lett. 102, 110–133.
Schiøtte, L., Hansen, B.T., Shirey, S.B., Bridgwater, D., 1993. Petrological and whole rock isotopic characteristics of tectonically juxtaposed Archaean gneisses in the Okay area of the Main Province, Labrador: relevance for terrane models. Precambrian Res. 63, 293–323.
Shaw, D.M., Cramer, J.J., Higgins, M.D., Truscott, M.G., 1986. Composition of the Canadian Precambrian shield and the continental crust of the Earth. Geol. Soc. Lond. Spec. Publ. 24, 275–282. https://doi.org/10.1144/GSL.SP.1986.024.01.24.
Siedenkrantz, M.-S., Kuijpers, A., Olsen, J., Pearce, C., Lindblom, S., Ploug, J., Przybylo, P., Snowball, I., 2019. Southwest Greenland shelf glaciation during MIS 4 more extensive than during the Last Glacial Maximum. Sci. Rep. 9, 15617. https://doi.org/10.1038/s41598-019-51983-3.
Sinha, A.K., Hogan, J.P., Parks, J., 1996. Lead isotope mapping of crustal reservoirs within the grenville superterrane: I. Central and southern appalachians. In: Basu, A.H., Stanley, R. (Eds.), Earth Processes: Reading the Isotopic Code. AGU, Washington, D. C, pp. 293–305.
Skinner, L.C., Shackleton, N.J., 2005. An Atlantic lead over Pacific deep-water change across Termination I: implications for the application of the marine isotope stage stratigraphy. QSR 24, 571–580.
Smith, P.E., 1988. U-Th-Pb Geochronology of Archean Rocks of the Eastern Superior Province and Application of Initial Pb and Hf Isotope Ratios to Greenstone Belt Evolution; Unpublished PhD Thesis. University of Toronto, Toronto, Ontario, p. 125.
Stevenson, R., Henry, P., Gariepy, C., 1999. Assimilation-fractional crystallization origin of archean sanukitoid suites: western superior Province, Canada. Precambrian Res. 96, 83–99.
Stokes, C.R., Tarasov, L., Dyke, A.S., 2012. Dynamics of the north American ice sheet complex during its inception and build-up to the last glacial maximum. QSR 50, 86–104.
Strelow, F.W.E., 1978. Distribution coefficients and anion-exchange behavior of some elements in hydrobromic nitric acid mixtures. Anal. Chem. 50 (9), 1359–1361.
Süfke, F., Gutjahr, M., Gilli, A., Anselmetti, F.S., Glur, L., Eisenhauer, A., 2019. Early stage weathering systematics of Pb and Nd isotopes derived from a high-Alpine Holocene lake sediment record. Chem. Geol. 507, 42–53. https://doi.org/10.1016/j.chemgeo.2018.12.026.
Süfke, F., Gutjahr, M., Keigwin, L.D., Reilly, B., Giosan, L., Lippold, J, 2022. Arctic drainage of Laurentide Ice Sheet meltwater throughout the past 14,700 years. Commun. Earth Environ. 3 (98), 1–11. https://doi.org/10.1038/s43247-022-00428-3.
Svendsen, J.I., Alexanderson, H., Astakhov, V.I., Demidov, I., Dowdeswell, J.A., Funder, S., Gataullin, V., Henriksen, M., Hjort, C., Houmark-Nielsen, M., Hubberten, H.W., 2004. Late Quaternary ice sheet history of northern Eurasia. Quat. Sci. Rev. 23, 1229–1271.
Taylor, S.R., McLennan, S.M., 1985. The Continental Crust: its Composition and Evolution. Blackwell, Oxford, p. 312.
Taylor, P.N., Upton, B.G.J., 1993. Contrasting Pb isotopic compositions in two intrusive complexes of the Gardar Magmatic Province of South Greenland. Chem. Geol. 104, 261–268.
Taylor, P.N., Moorbath, S., Goodwin, R., Petrykowski, A.C., 1980. Crustal contamination as an indicator of the extent of early Archaean crust: Pb isotopic evidence from the late Archaean gneisses of West Greenland. Geochim. Cosmochim. Acta. 44, 1437–1453.
Taylor, P.N., Jones, N.W., Moorbath, S., 1984. Isotopic assessment of relative contributions from crust and mantle sources to the magma genesis of precambrian granitoid rocks. Phil. Trans. Roy. Soc. Lond. Math. Phys. Sci. 310 (1514), 605–625.
Taylor, P.N., Kalsbeek, F., Bridgwater, D., 1992. Discrepancies between neodymium, lead and strontium model ages from the Precambrian of southern East Greenland: evidence for a Proterozoic granulite-facies event affecting archaean gneisses. Chem. Geol. 94, 281–291.
Taylor, R.N., Ishizuka, O., Michalik, A., Milton, J.A., Croudace, I.W., 2015. Evaluating the precision of Pb isotope measurement by mass spectrometry. J. Anal. At. Spectrom. 30, 198–213.
Thorpe, R.I., 1982. Lead isotope evidence regarding archean and proterozoic metallogeny in Canada. Revista Brasileira de Geosciencias 12 (1–2), 510–521.
Thorpe, R.I., 2008. Release of lead isotope data in 4 databases: Canadian, Western Superior, foreign, and whole rock and feldspar. GSC Open file 5664.
Thrane, K., 2004. Palaeoproterozoic age of a basement gneiss complex in the Charcot Land tectonic window, East Greenland Caledonides. In: Higgins, A.K.,

Kalsbeek, F. (Eds.), East Greenland Caledonides: Stratigraphy, Structure and Geochronology, vol. 6. Geological Survey of Denmark and Greenland Bulletin.
Geology of Ontario. In: Thurston, P.C., Williams, H.R., Sutcliffe, R.H., Stott, G.M. (Eds.), Ontario Geol. Surv. Stud. 4.
Vance, D., Teagle, D.A.H., Foster, G.L., 2009. Variable Quaternary chemical weathering fluxes and imbalances in marine geochemical budgets. Nature 458, 493–496. https://doi.org/10.1038/nature07928.
Vervoort, J.D., White, W.M., Thorpe, R.I., Franklin, J.M., 1993. Postmagmatic thermal activity in the Abitibi Greenstone Belt, Noranda and Matagami districts: evidence from whole-rock Pb isotope data. Econ. Geol. 88, 1598–1614.
Wadham, J.L., Tranter, M., Skidmore, M., Hodson, A.J., Priscu, J., Lyons, W.B., Sharp, M., Wynn, P., Jackson, M., 2010. Biogeochemical weathering under ice: Size matters. Global Biogeochem. Cycles 24 (3), GB3025. https://doi.org/10.1029/2009GB003688.
Wainer, K.A.I., Rowe, M.P., Thomas, A.L., Mason, A.J., Williams, B., Tamisiea, M.E., Williams, F.H., Dusterhus, A., Henderson, G.M., 2017. Speleothem evidence for MIS 5c and 5a sea level above modern level at Bermuda. Earth Planet Sci. Lett. 457, 325–334.
Wedepohl, K.H., Heinrichs, H., Bridgwater, D., 1991. Chemical characteristics and genesis of the quartz-feldspathic rocks in the Archean crust of Greenland. Contrib. Mineral. Petrol. 107, 163–179. https://doi.org/10.1007/BF00310705.
White, L.E., Bailey, I., Foster, G.L., Georgina, A., Kelley, S.P., Andrews, J.T., Hogan, K., Dowdeswell, J.A., Storey, C.D., 2016. Tracking the provenance of Greenland-sourced, Holocene aged individual sand-sized ice-rafted debris using the Pb-isotope composition of feldspars and 40Ar/39Ar ages of hornblendes. Earth Planet Sci. Lett. 433, 192–203.
Wu, T., Polat, A., Frei, R., Fryer, B.J., Yang, K.-G., Kusty, T., 2016. Geochemistry, Nd, Pb and Sr isotope systematics, and U-Pb zircon ages of the Neoarchean Bad Vermillion Lake greenstone belt and spatially associated granitic rocks, western Superior Province, Canada. Precambrian Res. 282, 21–51. https://doi.org/10.1016/j.precamres.2016.06.021.
Zheng, X.-Y., Plancherel, Y., Saito, M.A., Scott, P.M., Henderson, G.M., 2016. Rare Earth elements (REEs) in the tropical South Atlantic and quantitative deconvolution of their non-conservative behavior. Geochim. Cosmochim. Acta177, 217–237. https://doi.org/10.1016/j.gca.2016.01.018.
Zhou, Y., McManus, J.F., Jacobel, A.W., Costa, K.M., Wang, S., Caraveo, B.A., 2021. Enhanced iceberg discharge in the western North Atlantic during all Heinrich events of the last glaciation. Earth Planet Sci. Lett. 564, 116910.